

# A MODEL REDUCTION APPROACH FOR INVERSE PROBLEMS WITH OPERATOR VALUED DATA

JÜRGEN DÖLZ\*, HERBERT EGGER†, AND MATTHIAS SCHLOTTBOM‡

**Abstract.** We study the efficient numerical solution of linear inverse problems with operator valued data which arise, e.g., in seismic exploration, inverse scattering, or tomographic imaging. The high-dimensionality of the data space implies extremely high computational cost already for the evaluation of the forward operator, which makes a numerical solution of the inverse problem, e.g., by iterative regularization methods, practically infeasible. To overcome this obstacle, we develop a novel model reduction approach that takes advantage of the underlying tensor product structure of the problem and which allows to obtain low-dimensional certified reduced order models of quasi-optimal rank. A complete analysis of the proposed model reduction approach is given in a functional analytic setting and the efficient numerical construction of the reduced order models as well as of their application for the numerical solution of the inverse problem is discussed. In summary, the setup of a low-rank approximation can be achieved in an offline stage at essentially the same cost as a single evaluation of the forward operator, while the actual solution of the inverse problem in the online phase can be done with extremely high efficiency. The theoretical results are illustrated by application to a typical model problem in fluorescence optical tomography.

**Key words.** Inverse problems, model reduction, low-rank approximation, matrix compression, singular value decomposition, hyperbolic cross approximation, optimal experiment design, fluorescence optical tomography

**AMS subject classifications.** 46N40, 65J20, 65N21

**1. Introduction.** We consider the efficient numerical solution of linear inverse problems with operator valued data modeled by abstract operator equations

$$(1.1) \quad \mathcal{T}c = \mathcal{M}^\delta.$$

We assume that  $\mathcal{M}^\delta : \mathbb{Y} \rightarrow \mathbb{Z}'$ , representing the possibly perturbed measurements, is a linear operator of Hilbert-Schmidt class between Hilbert spaces  $\mathbb{Y}$  and  $\mathbb{Z}'$ , the dual of  $\mathbb{Z}$ . We further assume that the forward operator  $\mathcal{T} : \mathbb{X} \rightarrow \text{HS}(\mathbb{Y}, \mathbb{Z}')$  is linear and compact, and admits a factorization of the form

$$(1.2) \quad \mathcal{T}c = \mathcal{V}' \mathcal{D}(c) \mathcal{U}.$$

Problems of this kind arise, for instance, as mathematical models for tomographic applications [1, 25] or inverse scattering problems [6, 13], and as linearizations of related nonlinear problems, see e.g., [8, 20, 29] or [20] and the references given there. In such applications,  $\mathcal{U}$  typically models the propagation of excitation fields generated by the sources,  $\mathcal{D}$  describes the interaction with the medium to be probed, and  $\mathcal{V}'$  models the emitted fields which can be recorded by the detectors. In the following, we briefly outline our basic approach towards the numerical solution of (1.1)–(1.2) and report about related work in the literature.

\*Department of Applied Mathematics, University of Twente, P.O. Box 217, 7500 AE Enschede, The Netherlands. [j.dolz@utwente.nl](mailto:j.dolz@utwente.nl)

†Numerical Analysis and Scientific Computing, Department of Mathematics, TU Darmstadt, Dolivostr. 15, 64293 Darmstadt, Germany. [egger@mathematik.tu-darmstadt.de](mailto:egger@mathematik.tu-darmstadt.de)

‡Department of Applied Mathematics, University of Twente, P.O. Box 217, 7500 AE Enschede, The Netherlands. [m.schlottbom@utwente.nl](mailto:m.schlottbom@utwente.nl)

**1.1. Regularized inversion.** Due to the special functional analytic setting, the inverse problem (1.1)–(1.2) amounts to an ill-posed linear operator equation in Hilbert spaces and standard regularization theory can be applied for its stable solution [2, 9]. Following the usual arguments, we assume that  $\mathcal{M}^\delta$  is a perturbed version of the exact data  $\mathcal{M}$  and that a bound on the measurement noise

$$(1.3) \quad \|\mathcal{M} - \mathcal{M}^\delta\|_{\mathbb{HS}(\mathbb{Y}, \mathbb{Z}')} \leq \delta$$

is available. We further denote by  $c^\dagger$  the minimum norm solution of (1.1) with  $\mathcal{M}^\delta$  replaced by  $\mathcal{M} = \mathcal{T}c^\dagger$ . A stable approximation for the solution  $c^\dagger$  can then be obtained by the regularized inversion of (1.1), e.g., via spectral regularization methods

$$(1.4) \quad c_\alpha^\delta = g_\alpha(\mathcal{T}^*\mathcal{T})\mathcal{T}^*\mathcal{M}^\delta = \mathcal{T}^*g_\alpha(\mathcal{T}\mathcal{T}^*)\mathcal{M}^\delta.$$

Here  $\mathcal{T}^* : \mathbb{HS}(\mathbb{Y}, \mathbb{Z}') \rightarrow \mathbb{X}$  denotes the adjoint of the operator  $\mathcal{T}$ . A typical choice of the filter function in this context is  $g_\alpha(\lambda) = (\lambda + \alpha)^{-1}$ , which leads to Tikhonov regularization  $c_\alpha^\delta = (\mathcal{T}^*\mathcal{T} + \alpha\mathcal{I})^{-1}\mathcal{T}^*\mathcal{M}^\delta$ ; we refer to [2, 9] for details.

For the actual computation of the regularized solution  $c_\alpha^\delta$ , a sufficiently accurate finite dimensional approximation of the operator  $\mathcal{T}$  is required, which is usually obtained by some discretization procedure; in the language of model order reduction, this is called the *truth* or *high-fidelity approximation* [3, 27]. In the following discussion, we will not distinguish between infinite dimensional operators and their truth approximations. We thus assume that  $\dim(\mathbb{X}) = m$  and  $\dim(\mathbb{Y}) = \dim(\mathbb{Z}) = k$ , with dimensions  $m, k$  typically very large, which is required to guarantee that the truth approximation is sufficiently accurate. We may then identify  $c$  with a vector in  $\mathbb{R}^m$ ,  $\mathcal{M}^\delta$  with a matrix in  $\mathbb{R}^{k \times k}$ , and  $\mathcal{T}$  with a 3-tensor in  $\mathbb{R}^{m \times k \times k}$  or a matrix in  $\mathbb{R}^{m \times k^2}$ .

**1.2. Related work.** The high dimensionality of the problem poses severe challenges for the numerical solution of the inverse problem (1.1)–(1.2) and different model reduction approaches have been proposed to reduce the computational complexity. These typically rely on the construction of certain low-rank approximations for the forward operator  $\mathcal{T}$  or its adjoint  $\mathcal{T}^*$ , e.g., by truncated singular value decomposition. For problems with regular geometries and constant coefficients, fast analytic singular value decompositions of linear operators have been used in [22] based on Fourier techniques. In general, the full assembly and decomposition of  $\mathcal{T}$  is, however, computationally prohibitive for many applications. Krylov subspace methods [16, 30] and randomized algorithms [14, 23] then provide alternatives that allow to construct approximate singular value decompositions using only a moderate number of evaluations of  $\mathcal{T}$  and its adjoint  $\mathcal{T}^*$ . By combining randomized singular value decompositions for subproblems associated to a single frequency in a recursive manner, approximate singular value decompositions have been constructed in [5] in the context of inverse medium problems. A particular strategy towards dimension reduction consists in reducing synthetically the number of sources. Such *simultaneous* or *encoded sources* have been used in various applications with a large number of excitations and detectors, e.g., geophysics [15, 19] and tomography [31]; see [28] for further references.

In a recent work [21], motivated by [20], the forward operator  $\mathcal{T}$  is assumed to be the Khatri-Rao product of the matrices corresponding to the adjoint operators  $\mathcal{U}^*$  and  $\mathcal{V}^*$  in our setting; this induces a similar structure to (1.2) if  $\mathcal{D}(c)$  amounts to a diagonal matrix with  $c$  on its diagonal. The Khatri-Rao product structure allows the efficient evaluation of  $\mathcal{T}^*\mathcal{T}$ , required for the solution of the inverse problem, using pre-computed low-rank approximations for  $\mathcal{U}\mathcal{U}^*$  and  $\mathcal{V}\mathcal{V}^*$ ; see also [18] for a survey on

tensor decompositions. The computational cost of the proposed reconstruction algorithms in [21] is still rather high and may be prohibitive for problems with distributed parameters. For a survey of model reduction techniques that aim to reduce the dimension of the parameter space and to accelerate the solution of the computational models let us refer to [3, 27].

The approach developed in this paper aims at systematically constructing approximations  $\mathcal{T}_N$  for the operator  $\mathcal{T}$  with a quasi-optimal low rank comparable to that of the truncated singular value decomposition while at the same time allowing for a more efficient construction and also guaranteeing provable approximation error bounds. After model reduction, even very high dimensional inverse problem can be solved in parts of a second. In the following, we outline our approach in more detail.

**1.3. Model reduction.** A possible and rather general strategy towards dimension reduction, which we also use in this paper, amounts to projection in data space

$$(1.5) \quad \mathcal{T}_N = \mathcal{Q}_N \mathcal{T},$$

where  $\mathcal{Q}_N$  is chosen as some orthogonal projection with finite rank  $N$ , which is the dimension of the range of  $\mathcal{Q}_N$ . Since we assume that  $\mathcal{T}$  is compact, we can approximate it by finite rank operators, i.e., we can choose  $N$  sufficiently large such that

$$(1.6) \quad \|\mathcal{Q}_N \mathcal{T} - \mathcal{T}\|_{\mathbf{X} \rightarrow \mathbf{HS}(\mathbf{Y}, \mathbf{Z}')} \leq \delta.$$

Note that typically  $N \ll m, k$ , where  $m, k$  are the dimensions of the truth approximation used for the computations. Let us recall that the approximation of minimal rank  $N$ , satisfying (1.6), is obtained by truncated singular value decomposition of the operator  $\mathcal{T}$ , which will serve as the benchmark in the following discussion.

For the stable and efficient numerical solution of the inverse problem (1.1)–(1.2), we may then consider the low-dimensional regularized approximation

$$(1.7) \quad c_{\alpha, N}^{\delta} = \mathcal{T}_N^* g_{\alpha}(\mathcal{T}_N \mathcal{T}_N^*) \mathcal{Q}_N \mathcal{M}^{\delta}.$$

As shown in [24], the low-rank approximation  $c_{\alpha, N}^{\delta}$  defined in (1.7) has essentially the same quality as the infinite dimensional approximation  $c_{\alpha}^{\delta}$ , as long as the perturbation bound (1.6) can be guaranteed. In the sequel, we therefore focus on the numerical realization of (1.7), which can be roughly divided into the following two stages:

- Setup of the approximations  $\mathcal{Q}_N$ ,  $\mathcal{T}_N^*$ , and  $\mathcal{T}_N \mathcal{T}_N^*$ . This compute intensive part can be done in an *offline stage* and the constructed approximations can be used for repeated solution of the inverse problem (1.1) for multiple data.
- Computation of the regularized solution (1.7). This *online stage*, which is relevant for the actual solution of (1.1), requires of the following three steps:

step	computations	complexity	memory
compression	$\mathcal{M}_N^{\delta} = \mathcal{Q}_N \mathcal{M}^{\delta}$	$Nk^2$	$Nk^2$
analysis	$z_{\alpha, N}^{\delta} = g_{\alpha}(\mathcal{T}_N \mathcal{T}_N^*) \mathcal{M}_N^{\delta}$	$N^2$	$N^2$
synthesis	$c_{\alpha, N}^{\delta} = \mathcal{T}_N^* z_{\alpha, N}^{\delta}$	$Nm$	$Nm$

For the complexity and memory estimates above, we assumed that  $\mathcal{T} \in \mathbb{R}^{m \times k \times k}$  is the truth approximation obtained after discretization. Let us note that the analysis step is completely independent of the large system dimension  $k, m$  of the truth approximation

and therefore the compression and synthesis step are the compute intensive parts in the online stage. If  $k^2 > m$ , which is the typical situation [5, 21], then the data compression turns out to be the most compute and memory expensive step.

**1.4. Tensor product compression.** To further reduce the memory cost of the data compression, we may exploit the particular structure (1.2) of the forward operator reflected in the tensor product structure of the measurement space  $\mathbb{HS}(\mathbb{Y}, \mathbb{Z}')$ . We define a tensor product projection operator

$$(1.8) \quad \mathcal{Q}_{K,K} \mathcal{M}^\delta = \mathcal{Q}'_{K,\mathcal{V}} \mathcal{M}^\delta \mathcal{Q}_{K,\mathcal{U}}$$

via two separate projections  $\mathcal{Q}_{K,\mathcal{U}}$ ,  $\mathcal{Q}_{K,\mathcal{V}}$  of rank  $K$  in the spaces  $\mathbb{Y}$  and  $\mathbb{Z}$  of sources and detectors. After defining  $\mathcal{U}_K = \mathcal{U} \mathcal{Q}_{K,\mathcal{U}}$  and  $\mathcal{V}_K = \mathcal{V} \mathcal{Q}_{K,\mathcal{V}}$ , which are again operators of rank  $K$ , we obtain a tensor product approximation

$$(1.9) \quad \mathcal{T}_{K,K} c = \mathcal{Q}_{K,K} \mathcal{T} c = \mathcal{V}'_K \mathcal{D}(c) \mathcal{U}_K$$

of the forward operator whose rank is  $K^2$ . In the spirit of [15, 19], the columns of the operators  $\mathcal{Q}_{K,\mathcal{U}}$  and  $\mathcal{Q}_{K,\mathcal{V}}$  could be interpreted as *optimal sources* and *detectors*; their choice and construction is also strongly related to *optimal experiment design* [26].

With similar arguments as before, we may choose  $K$  sufficiently large such that

$$(1.10) \quad \|\mathcal{T}_{K,K} - \mathcal{T}\|_{\mathbb{X} \rightarrow \mathbb{HS}(\mathbb{Y}, \mathbb{Z}')} \leq \delta,$$

which yields a corresponding low-dimensional approximation  $c_{\alpha,K,K}^\delta$  for the regularized solution of (1.1) with still optimal approximation properties [24]. Further note that the tensor product structure of  $\mathcal{Q}_{K,K}$  allows to compute the projected data

$$\mathcal{M}_{K,K}^\delta = (\mathcal{Q}'_{K,\mathcal{V}} \mathcal{M}^\delta) \mathcal{Q}_{K,\mathcal{U}}$$

in two steps and that the first projection  $\mathcal{Q}'_{K,\mathcal{V}}$  can be applied already during recording of the data. Simultaneous access to the full data  $\mathcal{M}^\delta$  is therefore never required and the memory cost of data recording and compression is thereby reduced to  $3Kk + K^2$ . If only  $K \lesssim N$  is required in (1.10), then this is substantially smaller than the memory cost for computing  $\mathcal{M}_N^\delta = \mathcal{Q}_N \mathcal{M}^\delta$  with a generic projection  $\mathcal{Q}_N$  which does not take advantage of the underlying tensor product structure. Similar projections  $\mathcal{U}_K$  and  $\mathcal{V}_K$  of  $\mathcal{U}$  and  $\mathcal{V}$  were also used in [21] to speed-up the data compression step.

**1.5. Recompression.** One major disadvantage coming with the tensor product projection  $\mathcal{Q}_{K,K}$  is its still relatively high rank  $K^2$ , which is typically much larger than the optimal rank achievable by truncated singular value decomposition. To overcome this, we employ another compression of  $\mathcal{T}_{K,K}$ , giving rise to a projection

$$(1.11) \quad \mathcal{Q}_N = \mathcal{P}_N \mathcal{Q}_{K,K}$$

with rank  $N$  that can be proven to be virtually the same as the optimal rank of the truncated singular value decomposition. In this way, we can combine the advantages of an almost optimal rank  $N$  approximation and the tensor product pre-compression of the data. It turns out that this two-step construction is also beneficial for the computation of the projections  $\mathcal{Q}_{K,\mathcal{U}}$ ,  $\mathcal{Q}_{K,\mathcal{V}}$ , and  $\mathcal{P}_N$  and the operators  $\mathcal{T}_N \mathcal{T}_N^*$  and  $\mathcal{T}_N^*$  in the offline phase. Our analysis reveals that actually only a hyperbolic cross approximation [7] for the tensor product approximation is required for the recompression, which substantially improves the computational complexity.

**1.6. Main contributions and outline of the paper.** We will present a complete analysis of the proposed model reduction approach in an infinite-dimensional functional analytic setting. Our results thus become independent of the underlying truth approximation, which is only used for the actual computations, and we obtain a *certified* reduced order model with guaranteed error bounds. In addition, we demonstrate that these models can be constructed at substantially lower cost than typical low-rank approximations obtained by approximate singular value decompositions.

The remainder of the manuscript is organized as follows: In [section 2](#), we discuss in detail the construction of  $\mathcal{Q}_N = \mathcal{P}_N \mathcal{Q}_{K,K}$  for problems of the form [\(1.2\)](#). Under mild assumptions on the mapping properties of the operators  $\mathcal{U}$ ,  $\mathcal{D}$ , and  $\mathcal{V}$ , we show how to define appropriate projections  $\mathcal{Q}_{K,\mathcal{U}}$ ,  $\mathcal{Q}_{K,\mathcal{V}}$ , and  $\mathcal{P}_N$  in order to rigorously establish the approximation property [\(1.6\)](#). In particular, we show how to construct the second projection  $\mathcal{P}_N$  in a post processing step that only requires access to the tensor product approximation  $\mathcal{T}_{K,K} = \mathcal{Q}_{K,K} \mathcal{T}$  or its hyperbolic cross approximation  $\mathcal{T}_K = \mathcal{Q}_K \mathcal{T}$ , but not to the full operator  $\mathcal{T}$ . To illustrate the applicability of our theoretical results, we discuss in [section 3](#) a particular example stemming from fluorescence diffuse optical tomography. An appropriate choice of function spaces allows us to verify all conditions required for the analysis of our approach. In [section 4](#), we report in detail about numerical tests, in which we demonstrate the computational efficiency of the model reduction approach and the resulting numerical solution of the inverse problems.

**2. Analysis of the model reduction approach.** We will start with introducing our basic notation and then provide a complete analysis of the data compression and model reduction approach outlined in the introduction.

**2.1. Notation.** Function spaces will be denoted by  $\mathbb{A}, \mathbb{B}, \dots$  and assumed to be separable Hilbert spaces with scalar product  $(\cdot, \cdot)_{\mathbb{A}}$  and norm  $\|\cdot\|_{\mathbb{A}}$ . By  $\mathbb{A}'$  we denote the dual of  $\mathbb{A}$ , i.e., the space of bounded linear functionals on  $\mathbb{A}$ , and by  $\langle a', a \rangle_{\mathbb{A}' \times \mathbb{A}}$  the corresponding duality product. Furthermore,  $\mathcal{L}(\mathbb{A}, \mathbb{B})$  denotes the Banach space of linear operators  $\mathcal{S} : \mathbb{A} \rightarrow \mathbb{B}$  with norm  $\|\mathcal{S}\|_{\mathcal{L}(\mathbb{A}, \mathbb{B})} = \sup_{\|a\|_{\mathbb{A}}=1} \|\mathcal{S}a\|_{\mathbb{B}} < \infty$ . We write  $\mathcal{R}(\mathcal{S}) = \{\mathcal{S}a : a \in \mathbb{A}\}$  for the range of the operator  $\mathcal{S}$  and define  $\text{rank}(\mathcal{S}) = \dim(\mathcal{R}(\mathcal{S}))$ . By  $\mathcal{S}' : \mathbb{B}' \rightarrow \mathbb{A}'$  and  $\mathcal{S}^* : \mathbb{B} \rightarrow \mathbb{A}$  we denote the dual and the adjoint of a bounded linear operator  $\mathcal{S} \in \mathcal{L}(\mathbb{A}, \mathbb{B})$  defined, respectively, for all  $a \in \mathbb{A}$ ,  $b \in \mathbb{B}$ , and  $b' \in \mathbb{B}'$  by

$$(2.1) \quad \langle \mathcal{S}'b', a \rangle_{\mathbb{A}' \times \mathbb{A}} = \langle b', \mathcal{S}a \rangle_{\mathbb{B}' \times \mathbb{B}} \quad \text{and} \quad (\mathcal{S}^*b, a)_{\mathbb{B}} = (b, \mathcal{S}a)_{\mathbb{A}}.$$

The two operators  $\mathcal{S}'$  and  $\mathcal{S}^*$  are directly related by Riesz-isomorphisms. Let us further recall that any compact linear operator  $\mathcal{S} : \mathbb{A} \rightarrow \mathbb{B}$  has a singular value decomposition, i.e., a countable system  $\{(\sigma_k, a_k, b_k)\}_{k \geq 1}$  such that

$$(2.2) \quad \mathcal{S}a = \sum_{k \geq 1} (a, a_k)_{\mathbb{A}} \sigma_k b_k,$$

with singular values  $\sigma_1 \geq \sigma_2 \geq \dots \geq 0$  and  $\{a_k : \sigma_k > 0\}$  and  $\{b_k : \sigma_k > 0\}$  denoting orthonormal basis for  $\mathcal{R}(\mathcal{S}^*) \subset \mathbb{A}$  and  $\mathcal{R}(\mathcal{S}) \subset \mathbb{B}$ , respectively. Also note that  $\|\mathcal{S}\|_{\mathcal{L}(\mathbb{A}, \mathbb{B})} = \sigma_1$  and  $\text{rank}(\mathcal{S}) = \sup\{k : \sigma_k > 0\}$ . Moreover, by the Courant-Fisher min-max principle [\[12\]](#), the  $(k+1)$ st singular value can be characterized by

$$(2.3) \quad \sigma_{k+1} = \min_{\mathbb{A}_k} \max_{a \in \mathbb{A}_k^\perp} \|\mathcal{S}a\|_{\mathbb{B}} / \|a\|_{\mathbb{A}},$$

where the  $\mathbb{A}_k$  denote  $k$ -dimensional subspaces of  $\mathbb{A}$ . Hence every linear compact operator  $\mathcal{S} : \mathbb{A} \rightarrow \mathbb{B}$  can be approximated by truncated singular value decompositions

$$(2.4) \quad \mathcal{S}_K a = \sum_{k \leq K} (a, a_k)_{\mathbb{A}} \sigma_k b_k,$$

with error  $\|\mathcal{S} - \mathcal{S}_K\|_{\mathcal{L}(\mathbb{A}, \mathbb{B})} = \sigma_{K+1}$ . Conversely, any linear bounded operator that can be approximated in norm by finite-rank operators is necessarily compact.

We further denote by  $\mathbb{HS}(\mathbb{A}, \mathbb{B}) \subset \mathcal{L}(\mathbb{A}, \mathbb{B})$  the Hilbert-Schmidt class of compact linear operators whose singular values are square summable. Note that  $\mathbb{HS}(\mathbb{A}, \mathbb{B})$  is a Hilbert space equipped with the scalar product  $(\mathcal{S}, \mathcal{R})_{\mathbb{HS}(\mathbb{A}, \mathbb{B})} = \sum_{k \geq 1} (\mathcal{S}a_k, \mathcal{R}a_k)_{\mathbb{B}}$ , where  $\{a_k\}_{k \geq 1}$  is an orthonormal basis of  $\mathbb{A}$ . Moreover, the scalar product and the associated norm are independent of the choice of this basis. Let us mention the following elementary results, which will be used several times later on.

LEMMA 2.1. (a) Let  $\mathcal{S} \in \mathbb{HS}(\mathbb{A}, \mathbb{B})$ . Then there exists a sequence  $\{\mathcal{S}_K\}_{K \in \mathbb{N}}$  of linear operators of rank  $K$ , such that  $\|\mathcal{S} - \mathcal{S}_K\|_{\mathcal{L}(\mathbb{A}, \mathbb{B})} \lesssim K^{-1/2}$ .

(b) Let  $\mathcal{S} : \mathbb{A} \rightarrow \mathbb{B}$ ,  $\mathcal{R} : \mathbb{B} \rightarrow \mathbb{C}$  be two linear bounded operators and at least one of them Hilbert-Schmidt. Then the composition  $\mathcal{R}\mathcal{S} : \mathbb{A} \rightarrow \mathbb{C}$  is Hilbert-Schmidt and

$$\begin{aligned} \|\mathcal{R}\mathcal{S}\|_{\mathbb{HS}(\mathbb{A}, \mathbb{C})} &\leq \|\mathcal{R}\|_{\mathcal{L}(\mathbb{B}, \mathbb{C})} \|\mathcal{S}\|_{\mathbb{HS}(\mathbb{A}, \mathbb{B})}, & \text{or} \\ \|\mathcal{R}\mathcal{S}\|_{\mathbb{HS}(\mathbb{A}, \mathbb{C})} &\leq \|\mathcal{R}\|_{\mathbb{HS}(\mathbb{B}, \mathbb{C})} \|\mathcal{S}\|_{\mathcal{L}(\mathbb{A}, \mathbb{B})}. \end{aligned}$$

Here and below, we use  $a \lesssim b$  to express  $a \leq Cb$  with some constant  $C$  that is irrelevant in the context, and we write  $a \simeq b$  when  $a \lesssim b$  and  $b \lesssim a$ .

For convenience of the reader, we provide a short proof of these assertions.

*Proof.* The assumption  $\mathcal{S} \in \mathbb{HS}(\mathbb{A}, \mathbb{B})$  implies that  $\mathcal{S}$  is compact with square summable singular values, and hence  $\sigma_{K, \mathcal{S}} \lesssim K^{-1/2}$ . The truncated singular value decomposition  $\mathcal{S}_K$  then satisfies  $\|\mathcal{S} - \mathcal{S}_K\|_{\mathcal{L}(\mathbb{A}, \mathbb{B})} \leq \sigma_{K, \mathcal{S}} \lesssim K^{-1/2}$  which yields (a). After choosing an orthonormal basis  $\{a_k\}_{k \geq 1} \subset \mathbb{A}$ , we can write

$$\begin{aligned} \|\mathcal{R}\mathcal{S}\|_{\mathbb{HS}(\mathbb{A}, \mathbb{C})}^2 &= \sum_k \|\mathcal{R}\mathcal{S}a_k\|_{\mathbb{C}}^2 \\ &\leq \|\mathcal{R}\|_{\mathcal{L}(\mathbb{B}, \mathbb{C})}^2 \sum_{k \geq 1} \|\mathcal{S}a_k\|_{\mathbb{B}}^2 = \|\mathcal{R}\|_{\mathcal{L}(\mathbb{B}, \mathbb{C})}^2 \|\mathcal{S}\|_{\mathbb{HS}(\mathbb{A}, \mathbb{B})}^2 \end{aligned}$$

which implies the first inequality of assertion (b). The second inequality follows from the same arguments applied to the adjoint  $(\mathcal{R}\mathcal{S})^* = \mathcal{S}^* \mathcal{R}^*$  and noting that the respective norms of an operator and its adjoint are the same.  $\square$

**2.2. Preliminaries and basic assumptions.** We now introduce in more detail the functional analytic setting for the inverse problem (1.1) used for our considerations. We assume that the operators  $\mathcal{U}$ ,  $\mathcal{V}$ ,  $\mathcal{D}$  appearing in definition (1.2) satisfy

*Assumption 2.2.* Let  $\mathcal{U} \in \mathbb{HS}(\mathbb{Y}, \mathbb{U})$ ,  $\mathcal{V} \in \mathbb{HS}(\mathbb{Z}, \mathbb{V})$ , and  $\mathcal{D} \in \mathcal{L}(\mathbb{X}, \mathcal{L}(\mathbb{U}, \mathbb{V}'))$ .

Following our convention, all function spaces appearing in these conditions, except the space  $\mathcal{L}(\cdot, \cdot)$ , are separable Hilbert spaces. We can now prove the following assertions.

LEMMA 2.3. Let *Assumption 2.2* be valid. Then  $\mathcal{T}(c) = \mathcal{V}' \mathcal{D}(c) \mathcal{U}$  defines a bounded linear operator  $\mathcal{T} : \mathbb{X} \rightarrow \mathbb{HS}(\mathbb{Y}, \mathbb{Z}')$  and, additionally,  $\mathcal{T}$  is compact.

*Proof.* Linearity of  $\mathcal{T}$  is clear by construction and the linearity of  $\mathcal{U}$ ,  $\mathcal{V}$ , and  $\mathcal{D}$ . Now let  $\{y_k\}_{k \geq 1}$  denote an orthonormal basis of  $\mathbb{Y}$  and let  $c \in \mathbb{X}$  be arbitrary. Then

$$\begin{aligned} \|\mathcal{T}c\|_{\mathbb{HS}(\mathbb{Y}, \mathbb{Z}')}^2 &= \sum_{k \geq 1} \|\mathcal{V}' \mathcal{D}(c) \mathcal{U} y_k\|_{\mathbb{Z}'}^2 \leq \|\mathcal{V}' \mathcal{D}(c)\|_{\mathcal{L}(\mathbb{U}, \mathbb{Z}')}^2 \sum_{k \geq 1} \|\mathcal{U} y_k\|_{\mathbb{U}}^2 \\ &\leq \|\mathcal{V}'\|_{\mathcal{L}(\mathbb{V}', \mathbb{Z}')}^2 \|\mathcal{D}\|_{\mathcal{L}(\mathbb{X} \rightarrow \mathcal{L}(\mathbb{U}, \mathbb{V}'))}^2 \|c\|_{\mathbb{X}}^2 \|\mathcal{U}\|_{\mathbb{HS}(\mathbb{Y}, \mathbb{U})}^2, \end{aligned}$$

where we used Lemma 2.1 in the second step, and the boundedness of the operators in the third. Since  $\|\mathcal{V}'\|_{\mathcal{L}(\mathbb{V}', \mathbb{Z}')} = \|\mathcal{V}\|_{\mathcal{L}(\mathbb{Z}, \mathbb{V})} \leq \|\mathcal{V}\|_{\mathbb{HS}(\mathbb{Z}, \mathbb{V})}$ , we obtain

$$\|\mathcal{T}c\|_{\mathbb{HS}(\mathbb{Y}, \mathbb{Z}')} \leq \|\mathcal{U}\|_{\mathbb{HS}(\mathbb{Y}, \mathbb{U})} \|\mathcal{V}\|_{\mathbb{HS}(\mathbb{Z}, \mathbb{V})} \|\mathcal{D}\|_{\mathcal{L}(\mathbb{X}, \mathcal{L}(\mathbb{U}, \mathbb{V}'))} \|c\|_{\mathbb{X}}$$

for all  $c \in \mathbb{X}$ , which shows that  $\mathcal{T}$  is bounded. Using Lemma 2.1(a), we can further approximate  $\mathcal{U}$  and  $\mathcal{V}$  by operators  $\mathcal{U}_K, \mathcal{V}_K$  of rank  $K$ , such that

$$(2.5) \quad \|\mathcal{U} - \mathcal{U}_K\|_{\mathcal{L}(\mathbb{Y}, \mathbb{U})} \lesssim K^{-1/2} \quad \text{and} \quad \|\mathcal{V} - \mathcal{V}_K\|_{\mathcal{L}(\mathbb{Z}, \mathbb{V})} \lesssim K^{-1/2},$$

and we can define an operator  $\mathcal{T}_{K,K} : \mathbb{X} \rightarrow \mathbb{HS}(\mathbb{Y}, \mathbb{Z}')$  by  $\mathcal{T}_{K,K}c = \mathcal{V}'_K \mathcal{D}(c) \mathcal{U}_K$ , which defines an approximation of  $\mathcal{T}$  of rank  $K^2$ . From Lemma 2.1(b), we infer that

$$\begin{aligned} \|\mathcal{T} - \mathcal{T}_{K,K}\|_{\mathcal{L}(\mathbb{X}, \mathbb{HS}(\mathbb{Y}, \mathbb{Z}'))} &= \sup_{\|c\|_{\mathbb{X}}=1} \|\mathcal{V}' \mathcal{D}(c) \mathcal{U} - \mathcal{V}'_K \mathcal{D}(c) \mathcal{U}_K\|_{\mathbb{HS}(\mathbb{Y}, \mathbb{Z}')} \\ &\leq (\|\mathcal{V}' - \mathcal{V}'_K\|_{\mathcal{L}(\mathbb{V}', \mathbb{Z}')} \|\mathcal{U}\|_{\mathbb{HS}(\mathbb{Y}, \mathbb{U})} + \|\mathcal{V}'\|_{\mathbb{HS}(\mathbb{V}', \mathbb{Z}')} \|\mathcal{U} - \mathcal{U}_K\|_{\mathcal{L}(\mathbb{Y}, \mathbb{U})}) \|\mathcal{D}\|_{\mathcal{L}(\mathbb{X}, \mathcal{L}(\mathbb{U}, \mathbb{V}'))}. \end{aligned}$$

Using Assumption 2.2 and the bounds (2.5), we thus conclude that  $\mathcal{T}$  can be approximated uniformly by finite-rank operators, and hence  $\mathcal{T}$  is compact.  $\square$

**2.3. Tensor product approximation.** As an immediate consequence of the arguments used in the previous theorem, we obtain the following approximation result.

LEMMA 2.4. *Let Assumption 2.2 hold. Then for any  $\delta > 0$  there exists  $K \in \mathbb{N}$  with  $K \lesssim \delta^{-2}$  and rank  $K$  approximations  $\mathcal{U}_K = \mathcal{U} \mathcal{Q}_{K,\mathcal{U}}$  and  $\mathcal{V}_K = \mathcal{V} \mathcal{Q}_{K,\mathcal{V}}$  such that*

$$(2.6) \quad \|\mathcal{U} - \mathcal{U}_K\|_{\mathcal{L}(\mathbb{Y}, \mathbb{U})} \leq \delta \quad \text{and} \quad \|\mathcal{V} - \mathcal{V}_K\|_{\mathcal{L}(\mathbb{Z}, \mathbb{V})} \leq \delta.$$

Here  $\mathcal{Q}_{K,\mathcal{U}}$  and  $\mathcal{Q}_{K,\mathcal{V}}$  are orthogonal projections on  $\mathbb{Y}$  and  $\mathbb{Z}$ , respectively. Furthermore, the operator  $\mathcal{T}_{K,K}$  defined by  $\mathcal{T}_{K,K}c = \mathcal{V}'_K \mathcal{D}(c) \mathcal{U}_K$  has rank  $K^2$  and satisfies

$$(2.7) \quad \|\mathcal{T} - \mathcal{T}_{K,K}\|_{\mathcal{L}(\mathbb{X}, \mathbb{HS}(\mathbb{Y}, \mathbb{Z}'))} \lesssim \delta.$$

If the singular values of  $\mathcal{U}$  and  $\mathcal{V}$  satisfy  $\sigma_{k,\mathcal{U}}, \sigma_{k,\mathcal{V}} \lesssim k^{-\alpha}$  for some  $\alpha > 1/2$ , then the assertions hold with  $K \simeq \delta^{-1/\alpha}$ , and consequently  $\text{rank}(\mathcal{T}_{K,K}) \lesssim \delta^{-2/\alpha}$ .

*Remark 2.5.* The operators  $\mathcal{U}_K$  and  $\mathcal{V}_K$  can be obtained by truncated singular value decomposition of  $\mathcal{U}$  and  $\mathcal{V}$ , and  $\mathcal{Q}_{K,\mathcal{U}}$  and  $\mathcal{Q}_{K,\mathcal{V}}$  then are the projections onto the spaces spanned by the first  $K$  right singular vectors of  $\mathcal{U}$  and  $\mathcal{V}$ , respectively. The assertions of the lemma further imply in particular that the singular values of  $\mathcal{T}$  decay at least like  $\sigma_{k,\mathcal{T}} \lesssim k^{-\beta}$  with  $\beta \geq \alpha/2 \geq 1/4$ ; the latter follows from the fact the  $\mathcal{U}$  and  $\mathcal{V}$  are Hilbert-Schmidt, and thus their singular values are square summable.

**Hyperbolic cross approximation.** Any operator  $\mathcal{S}_\delta : \mathbb{A} \rightarrow \mathbb{B}$  for  $\mathcal{S} : \mathbb{A} \rightarrow \mathbb{B}$  with  $\|\mathcal{S} - \mathcal{S}_\delta\|_{\mathcal{L}(\mathbb{A}, \mathbb{B})} \lesssim \delta$  will be called a  $\delta$ -approximation for  $\mathcal{S}$  in the following. Note that  $\mathcal{T}_{K,K} = \mathcal{Q}_{K,K} \mathcal{T}$  is a  $\delta$ -approximation of rank  $K^2$ , while the  $\delta$ -approximation of minimal rank is obtained by truncated singular value decomposition (2.4). In particular, this implies that  $\text{rank}(\mathcal{T}_N) \lesssim \text{rank} \mathcal{T}_{K,K}$ . We will illustrate now, that the converse statement is in general not true, i.e., the tensor product approximation  $\mathcal{T}_{K,K}$  may have substantially higher rank than required for the  $\delta$ -approximation property.

LEMMA 2.6. *Let  $\sigma_{k,\mathcal{U}} \lesssim k^{-\beta}$  and  $\sigma_{k,\mathcal{V}} \lesssim k^{-\alpha}$  for some  $\beta > 1/2$  and  $\alpha > \beta + 1/2$ . Then we have  $\sigma_{k,\mathcal{T}} \lesssim k^{-\beta}$ , and for any  $\delta > 0$ , we can find  $N \in \mathbb{N}$  with  $N \lesssim \delta^{-1/\beta}$  and an approximation  $\mathcal{T}_N = \mathcal{Q}_N \mathcal{T}$  of rank  $N$ , such that*

$$(2.8) \quad \|\mathcal{T} - \mathcal{T}_N\|_{\mathcal{L}(\mathbb{X}, \mathbb{HS}(\mathbb{Y}, \mathbb{Z}'))} \lesssim \delta.$$

*Proof.* Let  $\{\sigma_{k,*}, a_{k,*}, b_{k,*}\}$  denote the singular systems for  $\mathcal{U}$  and  $\mathcal{V}'$ , respectively. We now show that the hyperbolic cross approximation [7]

$$\mathcal{T}_N c = \sum_{k \geq 1} \sum_{\ell=1}^{N_k} \sigma_{\ell,\mathcal{U}} \sigma_{k,\mathcal{V}'} (\cdot, a_{\ell,\mathcal{U}})_{\mathbb{Y}} \langle \mathcal{D}(c) b_{\ell,\mathcal{U}}, a_{k,\mathcal{V}'} \rangle_{\mathbb{V}' \times \mathbb{V}} b_{k,\mathcal{V}'},$$



with the choice  $N_k = \lfloor N/k^{1+\epsilon} \rfloor$ ,  $N \simeq \delta^{-1/\beta}$ , and  $\epsilon = (\alpha - \beta - 1/2)/(2\beta) > 0$  has the required properties. By counting, one can verify that  $\text{rank}(\mathcal{T}_N) \lesssim \sum_{k \geq 1} N_k \lesssim N$ , since by construction  $N_k \simeq N/k^{1+\epsilon}$  is summable. Furthermore, we can bound

$$\begin{aligned} \|\mathcal{T}c - \mathcal{T}_N c\|_{\mathbb{HS}(\mathbb{U}, \mathbb{V}')}^2 &= \sum_{m \geq 1} \|(\mathcal{T}c - \mathcal{T}_N c)a_{m, \mathcal{U}}\|_{\mathbb{V}'}^2 \\ &= \sum_{k \geq 1} \sigma_{k, \mathbb{V}'}^2 \left| \sum_{\ell \geq N_k + 1} \sigma_{\ell, \mathcal{U}} \langle \mathcal{D}(c)b_{\ell, \mathcal{U}}, a_{k, \mathbb{V}'} \rangle_{\mathbb{V}' \times \mathbb{V}} \right|^2 \\ &\leq \sum_{k \geq 1} \sigma_{k, \mathbb{V}'}^2 \sigma_{N_k}^2 \|\mathcal{D}(c)\|_{\mathcal{L}(\mathbb{U}, \mathbb{V}')}^2 \|a_{k, \mathbb{V}'}\|_{\mathbb{V}'}^2. \end{aligned}$$

By observing that  $\|a_{k, \mathbb{V}'}\|_{\mathbb{V}'} = 1$ ,  $\|\mathcal{D}(c)\|_{\mathcal{L}(\mathbb{U}, \mathbb{V}')} \lesssim \|c\|_{\mathbb{X}}$ , and  $\sigma_{k, \mathbb{V}'} = \sigma_{k, \mathbb{V}}$  and by using the decay properties of the singular values, we obtain

$$\|\mathcal{T} - \mathcal{T}_N\|_{\mathcal{L}(\mathbb{X}, \mathbb{HS}(\mathbb{U}, \mathbb{V}'))}^2 \lesssim \sum_{k \geq 1} k^{-2\alpha + 2\beta(1+\epsilon)} N^{-2\beta} \lesssim \delta^2.$$

In the last step, we used the fact that  $-2\alpha + 2\beta(1+\epsilon) < -1$  and  $N \simeq \delta^{-1/\beta}$ , which follows immediately from the construction.  $\square$

*Remark 2.7.* Comparing the results of [Lemmas 2.4](#) and [2.6](#), we expect to obtain a tensor product approximation  $\mathcal{T}_{K, K}$  of rank  $K^2 \simeq \delta^{-\alpha/2}$  while the hyperbolic cross approximation  $\mathcal{T}_N$  and consequently also the truncated singular value decomposition of the same accuracy only have rank  $N \lesssim \delta^{-\alpha+1/2+\epsilon}$ , which may be substantially smaller for  $\alpha > 1$ . Hence the rank of the tensor product approximation  $\mathcal{T}_{K, K}$  will, in general, not be of optimal order.

**2.4. Quasi-optimal low-rank approximation via recompression.** We will now show that a further compression of the tensor product approximation  $\mathcal{T}_{K, K}$  allows to obtain a low-rank approximation  $\mathcal{T}_N$  with quasi-optimal rank.

**LEMMA 2.8.** *Let  $\delta > 0$  and  $\mathcal{T}_{K, K} = \mathcal{V}'_K \mathcal{D}(\cdot) \mathcal{U}_K$  denote a  $\delta$ -approximation for  $\mathcal{T}$  according to [Lemma 2.4](#). Further assume that the singular values of  $\mathcal{T}$  decay like*

$$(2.9) \quad \sigma_{k, \mathcal{T}} \lesssim k^{-\beta}, \quad \beta > 0.$$

*Then there exists an orthogonal projection  $\mathcal{P}_N$  on  $\mathbb{HS}(\mathbb{Y}, \mathbb{Z}')$  with rank  $N \lesssim \delta^{-1/\beta}$  and*

$$(2.10) \quad \|\mathcal{T} - \mathcal{P}_N \mathcal{T}_{K, K}\|_{\mathcal{L}(\mathbb{X}, \mathbb{HS}(\mathbb{Y}, \mathbb{Z}'))} \lesssim \delta.$$

*Moreover,  $\mathcal{P}_N$  can be constructed using only knowledge of the approximation  $\mathcal{T}_{K, K}$ .*

*Proof.* For ease of notation, we use  $\|\cdot\| = \|\cdot\|_{\mathcal{L}(\mathbb{X}, \mathbb{HS}(\mathbb{Y}, \mathbb{Z}'))}$  to abbreviate the corresponding operator norm. Now let  $\mathcal{P}_{N, \mathcal{T}}$  denote the truncated singular value decomposition of  $\mathcal{T}$  with rank  $N \simeq \delta^{-1/\beta}$ . Using assumption [\(2.9\)](#) we obtain that

$$\|\mathcal{P}_{N, \mathcal{T}} \mathcal{T} - \mathcal{T}\| = \sigma_{N+1, \mathcal{T}} \lesssim \delta.$$

Furthermore, let  $\mathcal{P}_N \mathcal{T}_{K, K}$  be the truncated singular value decomposition of  $\mathcal{T}_{K, K}$  with the same rank  $N$  as above. Then by the triangle inequality

$$\|\mathcal{T} - \mathcal{P}_N \mathcal{T}_{K, K}\| \leq \|\mathcal{T} - \mathcal{T}_{K, K}\| + \|\mathcal{T}_{K, K} - \mathcal{P}_N \mathcal{T}_{K, K}\|.$$

The first term can be bounded using the  $\delta$ -approximation property of  $\mathcal{T}_{K, K}$ . From the min-max characterization of the singular values [\(2.3\)](#), we know that the truncated singular value decomposition yields the best-approximation in the set of bounded



linear operators with rank  $\leq N$ ; also known as the Eckart-Young-Mirsky theorem. Hence the second term can be further estimated by

$$\begin{aligned} \|(\mathcal{I} - \mathcal{P}_N)\mathcal{T}_{K,K}\| &\leq \|(\mathcal{I} - \mathcal{P}_{N,\mathcal{T}})\mathcal{T}_{K,K}\| \\ &\leq \|(\mathcal{I} - \mathcal{P}_{N,\mathcal{T}})\mathcal{T}\| + \|(\mathcal{I} - \mathcal{P}_{N,\mathcal{T}})(\mathcal{T} - \mathcal{T}_{K,K})\| \\ &\leq \sigma_{N+1,\mathcal{T}} + \|\mathcal{T} - \mathcal{T}_{K,K}\| \lesssim \delta. \end{aligned}$$

Here we used that  $\|\mathcal{I} - \mathcal{P}_{N,\mathcal{T}}\|_{\mathbb{HS}(\mathbb{Y},\mathbb{Z}')} \leq 1$  and the  $\delta$ -approximation property of  $\mathcal{T}_{K,K}$ . The result then follows by combination of the two estimates derived above.  $\square$

*Remark 2.9.* In the previous lemma, we could use instead of  $\mathcal{T}_{K,K}$  also any other  $\delta$ -approximation of the operator  $\mathcal{T}$ , e.g., the hyperbolic cross approximation constructed in Lemma 2.6; the proof carries over verbatim. In fact, the lemma relies on a well-known result from perturbation theory [17], viz., the singular values of the  $\delta$ -approximation  $\mathcal{T}_{K,K}$  are in a  $\delta$ -neighborhood of the singular values of  $\mathcal{T}$ .

**2.5. Summary.** Let us briefly summarize the main observations and results of this section. We constructed a certified reduced order model  $\mathcal{T}_N$ , i.e.,  $\delta$ -approximation, for the operator  $\mathcal{T}$  with quasi-optimal rank  $N$  comparable to that of truncated singular value decomposition. The given construction is based on certified low-rank approximations  $\mathcal{U}_K, \mathcal{V}_K$  for the operators  $\mathcal{U}$  and  $\mathcal{V}$  which can be computed more efficiently than a low-rank approximation for the full operator  $\mathcal{T} = \mathcal{V}'\mathcal{D}(\cdot)\mathcal{U}$ . The resulting tensor product approximation  $\mathcal{T}_{K,K}$  can then be further compressed by truncated singular value decomposition yielding the quasi-optimal low-rank approximation  $\mathcal{T}_N$ .

As can be seen from the proof of Lemma 2.6 and Remark 2.9, the tensor product approximation  $\mathcal{T}_{K,K}$  is not really needed but can be replaced by its hyperbolic cross approximation  $\mathcal{T}_K$  when computing the final approximation  $\mathcal{T}_N$ . This allows to substantially improve the computational complexity of the offline phase and is a key ingredient for the efficient realization of our model reduction approach.

The analysis in this section is done in abstract spaces and applies verbatim to infinite-dimensional operators as well as to their finite-dimensional truth approximations obtained after discretization. As a consequence, the computational results, e.g., the rank  $K$  and  $N$  of the approximations, can be expected to be essentially independent of the actual truth approximation used for computations.

**3. Fluorescence optical tomography.** In order to illustrate the viability of the theoretical results derived in the previous section, we now consider in some detail a typical application arising in medical imaging.

**3.1. Model equations.** Fluorescence optical tomography aims at retrieving information about the concentration  $c$  of a fluorophore inside an object by illuminating this object from outside with near infrared light and measuring the light reemitted by the fluorophores at a different wavelength. The distribution  $u_x = u_x(q_x)$  of the light intensity inside the object generated by a source  $q_x$  at the boundary, is described by

$$(3.1) \quad -\nabla \cdot (\kappa_x \nabla u_x) + \mu_x u_x = 0, \quad \text{in } \Omega,$$

$$(3.2) \quad \kappa_x \partial_n u_x + \rho_x u_x = q_x, \quad \text{on } \partial\Omega.$$

We assume that  $\Omega \subset \mathbb{R}^d$ ,  $d = 2, 3$ , is a bounded domain with smooth boundary enclosing the object under consideration. The light intensity  $u_m = u_m(u_x, c)$  emitted by the fluorophores is described by a similar equation

$$(3.3) \quad -\nabla \cdot (\kappa_m \nabla u_m) + \mu_m u_m = c u_x, \quad \text{in } \Omega,$$

$$(3.4) \quad \kappa_m \partial_n u_m + \rho_m u_m = 0, \quad \text{on } \partial\Omega.$$

The model parameters  $\kappa_i$ ,  $\mu_i$ , and  $\rho_i$ ,  $i = x, m$ , characterize the optical properties of the medium at excitation and emission wavelength; we assume these parameters to be known, e.g., determined by independent measurements [1]. As shown in [8], the above linear model, which can be interpreted as a Born approximation or linearization, is a valid approximation for moderate fluorophore concentrations.

**3.2. Forward operator.** The forward problem in fluorescence optical tomography models an experiment in which the emitted light resulting from excitation with a known source and after interaction with a given fluorophore concentration is measured at the boundary. The measurable quantity is the outward photon flux, which is proportional to  $u_m$ ; see [1] for details. The potential data for a single excitation with source  $q_x$  measured by a detector with characteristic  $q_m$  can be described by

$$(3.5) \quad \langle (\mathcal{T}c)q_x, q_m \rangle = \int_{\partial\Omega} u_m q_m ds(x),$$

where  $u_m$  and  $u_x$  are determined by the boundary value problems (3.1)–(3.4). The inverse problem finally consists of determining the concentration  $c$  of the fluorophore marker from measurements  $\langle \mathcal{T}(c)q_x, q_m \rangle$  for multiple excitations  $q_x$  and detectors  $q_m$ .

We now illustrate that fluorescence optical tomography perfectly fits into the abstract setting of section 2. Let us begin with defining the excitation operator

$$(3.6) \quad \mathcal{U} : H^1(\partial\Omega) \rightarrow H^1(\Omega), \quad q_x \mapsto \mathcal{U}q_x := u_x,$$

which maps a source  $q_x$  to the corresponding weak solution  $u_x$  of (3.1)–(3.2). The interaction with the fluorophore can be described by the multiplication operator

$$(3.7) \quad \mathcal{D} : L^2(\Omega) \rightarrow \mathcal{L}(H^1(\Omega), H^1(\Omega)'), \quad \mathcal{D}(c)u = cu.$$

In dimension  $d \leq 3$ , the product  $cu$  of two functions  $c \in L^2(\Omega)$  and  $u \in H^1(\Omega)$ , lies in  $L^{3/2}(\Omega)$  and can thus be interpreted as a bounded linear functional on  $H^1(\Omega)$ ; this shows that  $\mathcal{D}$  is a bounded linear operator. We further introduce the linear operator

$$(3.8) \quad \mathcal{V} : H^1(\partial\Omega) \rightarrow H^1(\Omega), \quad q_m \mapsto \mathcal{V}q_m := v_m,$$

which maps  $q_m$  to the weak solution  $v_m$  of the adjoint emission problem

$$(3.9) \quad -\nabla \cdot (\kappa_m \nabla v_m) + \mu_m v_m = 0, \quad \text{in } \Omega,$$

$$(3.10) \quad \kappa_m \partial_n v_m + \rho_m v_m = q_m, \quad \text{on } \partial\Omega.$$

One can verify that  $\mathcal{V}$  is the dual of the solution operator  $u_m|_{\partial\Omega} = \mathcal{V}'\mathcal{D}(c)u_x$  of the system (3.3)–(3.4); see [8] for details. Hence we may express the forward operator as

$$(3.11) \quad \mathcal{T}c = \mathcal{V}'\mathcal{D}(c)\mathcal{U}.$$

As function spaces we choose  $\mathbb{U} = \mathbb{V} = H^1(\Omega)$ ,  $\mathbb{Y} = \mathbb{Z} = H^1(\partial\Omega)$ , and  $\mathbb{X} = L^2(\Omega)$ .

In order to apply the results of section 2, it remains to verify Assumption 2.2. We already showed that  $\mathcal{D} \in \mathcal{L}(\mathbb{X}, \mathcal{L}(\mathbb{U}, \mathbb{V}'))$  is a bounded linear operator. The following assertion states that also the remaining conditions on  $\mathcal{U}$  and  $\mathcal{V}$  hold true.

**LEMMA 3.1.** *The operators  $\mathcal{U}$  and  $\mathcal{V}$  defined in (3.6) and (3.8) are Hilbert-Schmidt and their singular values decay like  $\sigma_{k,\mathcal{U}} \lesssim k^{-3/(2d-2)}$  and  $\sigma_{k,\mathcal{V}} \lesssim k^{-3/(2d-2)}$ .*

*Proof.* The Hilbert-Schmidt property follows immediately from the decay behavior of the singular values. To show the latter, let  $\mathbb{Y}_h = P_1(\mathcal{T}_h) \cap H^1(\partial\Omega) \subset H^{-1/2}(\partial\Omega)$  be the space of piecewise linear finite elements on a quasi-uniform triangulation  $\mathcal{T}_h$  of  $\partial\Omega$  with meshsize  $h$ . Let  $\mathcal{Q}_h$  be the  $L^2$ -orthogonal projection onto  $\mathbb{Y}_h$  and  $q \in H^1(\partial\Omega)$  arbitrary. Then standard approximation error estimates, see e.g., [4], yield

$$\|q - \mathcal{Q}_h q\|_{H^{-1/2}(\partial\Omega)} \lesssim h^{3/2} \|q\|_{H^1(\partial\Omega)}.$$

A-priori estimates for elliptic PDEs yield  $\|\mathcal{U}q\|_{H^1(\Omega)} \lesssim \|q\|_{H^{-1/2}(\partial\Omega)}$ , and hence  $\mathcal{U}$  can be continuously extended to an operator on  $H^{-1/2}(\partial\Omega)$ ; see e.g. [10]. This yields

$$\|\mathcal{U} - \mathcal{U}\mathcal{Q}_h\|_{\mathcal{L}(H^{-1/2}(\partial\Omega), H^1(\Omega))} \lesssim h^{3/2} \lesssim k^{-3/(2d-2)},$$

where  $k = \dim(\mathbb{Y}_h) = \text{rank}(\mathcal{Q}_h) \simeq h^{-(d-1)}$  is the dimension of the space  $\mathbb{Y}_h$ . From the min-max characterization of the singular values (2.3), we may therefore conclude that  $\sigma_{k,\mathcal{U}} \lesssim k^{-3/(2d-2)}$  as required. The result for  $\sigma_{k,\mathcal{V}}$  follows in the same way.  $\square$

*Remark 3.2.* If prior knowledge  $\text{supp}(c) \subset \Omega$  on the support of the fluorophore concentration is available, which is frequently encountered in practice, elliptic regularity [10] implies exponential decay of the singular values  $\sigma_{k,\mathcal{U}}$  and  $\sigma_{k,\mathcal{V}}$ . In such a situation, the rank  $K$  and  $N$  in Lemmas 2.4 and 2.8 will depend only logarithmically on the noise level  $\delta$ , and an accurate approximation  $\mathcal{T}_N$  of very low rank can be found.

**4. Numerical illustration.** We will now discuss in detail the implementation of the model reduction approach presented in section 2 for the fluorescence optical tomography problem and demonstrate its viability by some numerical tests.

**4.1. Truth approximation.** Let  $\mathcal{T}_h$  denote a quasi-uniform conforming triangulation of the domain  $\Omega$  with  $h > 0$  denoting the mesh size. For the discretization of (3.1)–(3.2) and (3.9)–(3.10), we use a standard finite element method with continuous piecewise linear polynomials; the corresponding spaces  $\mathbb{U}_h, \mathbb{V}_h \subset H^1(\Omega)$  then have dimension  $m \simeq h^{-d}$  each. We choose the same finite element space  $\mathbb{X}_h$  also for the approximation of the concentration  $c$ . The sources  $q_x, q_m$  for the forward and the adjoint problem are approximated by piecewise linear functions on the boundary of the same mesh  $\mathcal{T}_h$ ; hence  $\mathbb{Y}_h, \mathbb{Z}_h \subset H^1(\partial\Omega)$  have dimension  $k \simeq h^{d-1}$ . All approximation spaces are equipped with the topologies induced by their infinite dimensional counterparts. Standard error estimates allow to quantify the discretization errors in the resulting truth approximation of the forward operator and to establish the  $\delta$ -approximation property for  $h$  small enough. The error introduced by the discretization can therefore be assumed to be negligible.

Let us briefly discuss in a bit more detail the algebraic structure of the resulting problems arising in the truth approximation. Choosing standard nodal bases, the finite element approximation of problem (3.1)–(3.2) leads to the linear system

$$(4.1) \quad (\mathbf{K}_x + \mathbf{M}_x + \mathbf{R}_x) \mathbf{U} = \mathbf{E}_x \mathbf{Q}_x.$$

Here  $\mathbf{K}_x, \mathbf{M}_x \in \mathbb{R}^{m \times m}$  are the stiffness and mass matrices with coefficients  $\kappa_x, \mu_x$ , and the matrices  $\mathbf{R}_x \in \mathbb{R}^{m \times m}$ ,  $\mathbf{E}_x \in \mathbb{R}^{m \times k}$  stem from the discretization of the boundary conditions. The columns of regular  $\mathbf{Q}_x \in \mathbb{R}^{k \times k}$  represent the individual independent sources in the basis of  $\mathbb{Y}_h$ . Any excitation generated by a source in  $\mathbb{Y}_h$  can thus be expressed as a linear combination of columns of the excitation matrix  $\mathbf{U} \in \mathbb{R}^{m \times k}$ , which serves as a discrete counterpart of the operator  $\mathcal{U}$ . In a similar manner, the

discretization of the adjoint problem (3.9)–(3.10) leads to

$$(4.2) \quad (K_m + M_m + R_m) V = E_m Q_m.$$

whose solution matrix  $V \in \mathbb{R}^{m \times k}$  can be interpreted as the discrete counterpart of the operator  $\mathcal{V}$ . The system matrices  $K_m$ ,  $M_m$ ,  $R_m$ , and  $E_m$  have a similar meaning as above, and the columns of  $Q_m$  represent the individual detector characteristics. The algebraic form of the truth approximation finally reads

$$(4.3) \quad T(c) = V^\top D(c) U,$$

where  $D(c) \in \mathbb{R}^{m \times m}$  is the matrix representation of the finite element approximation for the operator  $\mathcal{D}(c_h)$  with  $c \in \mathbb{R}^m$  denoting the coordinates of the function  $c_h \in \mathbb{X}_h$ . The discrete measurement  $M_{ij} = (V^\top D(c) U)_{ij} = V(:, i)^\top D(c) U(:, j)$  then approximates the data taken by the  $i$ th detector for excitation with the  $j$ th source.

*Remark 4.1.* Let  $SY, SZ$  be the matrix representation of the  $H^1(\partial\Omega)$  inner products for the spaces  $\mathbb{Y}_h, \mathbb{Z}_h$ . Furthermore, let  $AY, AZ \in \mathbb{R}^{k \times k}$  be orthogonal with respect to  $SY$  and  $SZ$ , i.e.,  $AY^\top * SY * AY = I$  and  $AZ^\top * SZ * AZ = I$ . Then  $AY = Qx * Ax$  and  $AZ = Qm * Am$  with  $Ax = Qx^{-1} * AY$  and  $Am = Qm^{-1} * AZ$ , and the Hilbert-Schmidt norm of the measurement matrix  $M = T(c)$  can be expressed by the Frobenius norm

$$\|M\|_{\text{HS}} := \|Am^\top * M * Ax\|_{\text{F}}$$

Note that we simply have  $\|M\|_{\text{HS}} := \|M\|_{\text{F}}$  if the columns of  $Qx$ ,  $Qm$  are chosen orthonormal with respect to the  $SY$  and  $SZ$  inner products right from the beginning. We will use this fact in our numerical tests below.

**4.2. Realization of the model reduction approach.** We employ the fluorescence tomography example outlined in the previous section to sketch the basic steps of an implementation of the model reduction approach developed in section 2. For clarity, we provide code snippets of a MATLAB implementation, which is also used for the numerical tests reported in the next section.

**4.2.1. Application of the forward operator.** We start with assembling the system matrices for the excitation and the adjoint emission problem

```
[Kx,Mx,Rx,Ex,Qx]=assemble_system(mesh,kx,mx,rx,qx);
[Km,Mm,Rm,Em,Qm]=assemble_system(mesh,km,mm,rm,qm);
```

The matrix representations of the operators  $U$  and  $V$  are then simply obtained by

```
U=solve(Kx+Mx+Rx,Ex*Qx);
V=solve(Km+Mm+Rm,Em*Qm);
```

where  $x=\text{solve}(A,b)$  computes the solution of the linear system  $Ax=b$ . In our tests, we will simply use  $\text{solve}=@(A,b) A \backslash b$ ; see [11] for the use of preconditioned iterative solvers in fluorescence optical tomography. For simplicity, we choose  $Qx$  and  $Qm$  as the identity matrices for our computations, which amounts to considering all possible independent sources and detectors. We further define shortcuts for the matrix representation of the multiplication operator  $D$  and the discrete forward operator  $T$

```
D=@(c) assemble_mult(mesh,c);
T=@(c) V'*D(c)*U;
```

Note that the definition of  $T(c)$  makes explicit use of the underlying tensor product structure which allows a computationally efficient realization; see [11] for details.

**4.2.2. Orthonormalization.** Let  $SX, SY, SZ$  be the Gram matrices representing the scalar products of the function spaces  $\mathbb{X}_h, \mathbb{Y}_h, \mathbb{Z}_h$ . As a next step, we compute the approximations for the singular value decompositions of the excitation and emission operators. For this, we recall that the right singular vectors of an operator  $\mathcal{U}$  correspond to the eigenvectors of  $\mathcal{U}^* \mathcal{U}$ . The singular value decompositions for the matrices  $U$  and  $V$  can thus be computed by the generalized eigenvalue decompositions

$$\begin{aligned} [Ax, Dx] &= \text{eigs}(U' * SX * U, SY); \\ [Am, Dm] &= \text{eigs}(V' * SX * V, SZ); \end{aligned}$$

Note that some slight modifications would be required here, if the source and detector matrices  $Qx$  and  $Qm$  would not be chosen as the identity matrices. The columns of  $Ax$  and  $Am$  are orthogonal with respect to the  $SY$  and  $SZ$  scalar product and thus define bases of the discrete source and detector spaces. After appropriate scaling, the columns can be assumed to be normalized such that  $Ax' * SY * Ax$  and  $Am' * SZ * Am$  equal the identity matrix. To simplify the subsequent discussion, we change the definition of the sources and detectors as well as of the excitation and emission matrices, and redefine the forward operator according to

$$\begin{aligned} Qx &= Qx * Ax; \quad U = U * Ax; \quad Qm = Qm * Am; \quad V = V * Am; \\ T &= \mathcal{O}(c) \quad V' * D(c) * U; \end{aligned}$$

The columns of  $Qx$  and  $Qm$  are now orthogonal with respect to the  $SY$  and  $SZ$  scalar products, and as a consequence, the Hilbert-Schmidt norm in the measurement space amounts to the Frobenius norm of  $M = T(c)$ ; see [Remark 4.1](#) for details.

**4.2.3. Low-rank approximations for  $U$  and  $V$ .** The eigenvalues computed in the decompositions above correspond to the square of the singular values of  $U$  and  $V$ . We here allow for different ranks in the approximation and define truncation indices

$$\begin{aligned} dx &= \text{diag}(Dx); \quad xKK = \text{find}(dx > \delta^2); \quad xK = \text{length}(xKK); \\ dm &= \text{diag}(Dm); \quad mKK = \text{find}(dm > \delta^2); \quad mK = \text{length}(mK); \end{aligned}$$

We could further set  $K = \max(xK, mK)$  to stay exactly with the notation used in [section 2](#). The low-rank approximations for  $U$  and  $V$  and the resulting tensor product approximation of the forward operator  $T(c)$  are then given by

$$\begin{aligned} QxK &= Qx(:, xKK); \quad UK = U(:, xKK); \\ QmK &= Qm(:, mKK); \quad VK = V(:, mKK); \\ TKK &= \mathcal{O}(c) \quad VK' * D(c) * UK; \end{aligned}$$

Observe that the measurements  $MKK = TKK(c)$  obtained by this approximation correspond to a sub-block of the full measurements, i.e.,  $MKK = M(mK, xK)$ .

**4.2.4. Hyperbolic cross approximation.** The proof of [Lemma 2.6](#) shows that we may replace the tensor product operator  $TKK(c)$  by the hyperbolic cross approximation  $TK(c)$ , which takes into account only the entries  $M(k, l) = MKK(k, l)$  of the measurements  $M = T(c)$  for indices  $k \cdot l \leq N \lesssim \delta^{-\beta}$ . In our computations, we actually replace  $N$  by  $K$ , i.e., we utilize the hyperbolic cross approximation  $TK(c)$  of  $TKK(c)$ . The assembly of the matrix representation  $AK$  for  $TK(c) = AK * c$  then reads

```
m=0;
for k=1:K
    for l=1:floor(K/k)
        m=m+1;
        AK(m,:)=(VK(:,k))' * UK(:,l)' * DD;
    end
end
```

Here,  $DD$  is a diagonal matrix representing the numerical integration on the computational domain. Let us note that  $AK$  and thus also the operator  $TK(c)$  do not have a tensor product structure any more; therefore the measurements  $MK=TK(c)$  are stored as a column vector rather than a matrix. The norm in the reduced measurement space then is the Euclidean norm for vectors. Also note that the construction of  $AK$  and  $TK$  only requires access to the matrices  $UK$  and  $VK$  defining the operator  $TKK$ .

**4.2.5. Final recompression.** The last step in our model reduction approach consists in a further compression of the hyperbolic cross approximation  $TK$  of the tensor product operator  $TKK$ ; cf. [subsection 2.4](#) for details. This can be realized by

```
AKt=DD\AK'; AKAKt=AK*AKt;
[VA,DA]=eigs(AKAKt,NK);
```

where  $NK=size(AK,1)$  is the number of terms used for the hyperbolic cross approximation. The recompression then consists of selecting the largest entries, i.e.,

```
N=find(diag(DA)>delta^2);
AN=AK*VA(:,N); ANt=DD\AN';
```

Matrix representations for the projection operators  $\mathcal{Q}_{K,K}$ ,  $\mathcal{P}_K$ , and  $\mathcal{P}_N$  corresponding to the tensor product, the hyperbolic cross, and the final approximation, can be assembled easily from the eigenvectors computed during the construction.

**4.3. Numerical results.** The applicability and benefits of the model reduction approach proposed and analyzed in the previous sections are shown through solving an inverse problem in fluorescence tomography outlined in [section 3](#).

**4.3.1. Problem setup.** For ease of presentation, we consider a simple two-dimensional test problem. Our observations, however, carry over almost verbatim also to three dimensional problems of similar dimensions. A sketch of the domain and the coarsest mesh used for our computations as well as the parameter  $c^\dagger$  to be identified are depicted in [Figure 4.1](#). The computational meshes used for the truth

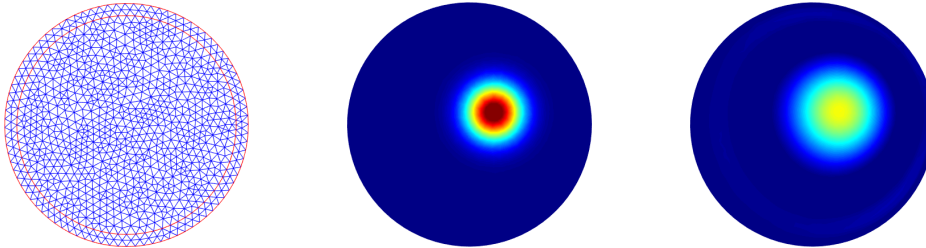


FIG. 4.1. *Left: computational domain and coarsest mesh used for our computations. Middle: minimum norm solution  $c^\dagger$ . Right: reconstructed fluorophore concentration  $c_\alpha^\delta$  for  $\delta = 10^{-5}$ .*

approximations are obtained by successive uniform refinement of the initial mesh. The characteristic dimension of the relevant function spaces after discretization can be deduced from [Table 4.1](#). For the finest mesh level  $ref=5$ , the discretized forward operator  $T$  amounts to a linear mapping from  $\mathbb{R}^{927161}$  to  $\mathbb{R}^{2816 \times 2816}$ . The storage of the matrix  $A$  representing the forward operator would require approximately 56TB of memory and even one single evaluation of  $T(c)$  via the matrix product  $Ac$  would require approximately 7Tflops. It should be clear that more sophisticated algorithms are required to make even the evaluation of the forward operator feasible.

TABLE 4.1

Dimensions  $m = \dim(\mathbb{X}_h) = \dim(\mathbb{U}_h) = \dim(\mathbb{V}_h)$  and  $k = \dim(\mathbb{Y}_h) = \dim(\mathbb{Z}_h)$  of the relevant function spaces after discretization for different refinement levels  $\text{ref}$  of the mesh. Note that  $m$  amounts to the overall number of mesh points while  $k$  is the number of boundary mesh points.

ref	0	1	2	3	4	5
$m$	993	3 881	15 345	61 025	243 393	927 161
$k$	88	176	352	704	1 408	2 816

**4.3.2. Tensor product representation.** From the particular form (4.3) of the forward operator, one can see that only the matrices  $\mathbf{U}$ ,  $\mathbf{V}$ , and a routine for the application of  $\mathbf{D}(\mathbf{c})$  are required to evaluate  $\mathbf{T}(\mathbf{c})$ . The application of  $\mathbf{D}(\mathbf{c})$  here amounts to the multiplication by a diagonal matrix which does not cause any significant overhead. In Table 4.2, we summarize the basic memory and computational cost for the required operations. Note that the matrices  $\mathbf{U}$  and  $\mathbf{V}$  can now be stored on a standard work-

TABLE 4.2

Memory requirements for the storage of the discretized operators  $\mathbf{U}$  and  $\mathbf{V}$  and operation count for the application of the forward operator  $\mathbf{T}(\mathbf{c}) = \mathbf{V}' * \mathbf{D}(\mathbf{c}) * \mathbf{U}$  using its tensor structure. The complexity estimates here are  $\text{mem} = 8(2km + m)$  bytes and  $\text{ops} = km + k^2m$  floating point operations.

ref	0	1	2	3	4	5
mem (T,GB)	0.001	0.010	0.080	0.640	5.106	40.793
ops (Tc, Gflop)	0.007	0.113	1.775	28.208	449.699	7 182.205

station, while the application of the forward operator is still too compute intensive to be useful for the efficient solution of the inverse problem under consideration.

Using multigrid solvers, the matrices  $\mathbf{U}$  and  $\mathbf{V}$  can be computed in  $O(mk)$  operations [11], which is, at least asymptotically, negligible compared to the application of  $\mathbf{T}(\mathbf{c})$  in tensor product form. In our computational tests, we utilize sparse direct solvers for the computation of  $\mathbf{U}$  and  $\mathbf{V}$ , for which the computational cost is  $O(m^{3/2} + km \log(m))$ . Since  $m^{3/2} \leq mk$  and  $\log(m) \leq k$  in our two-dimensional setting, this is still of lower complexity than even a single evaluation of  $\mathbf{T}(\mathbf{c})$ .

**4.3.3. Model reduction – offline phase.** The first step of our model reduction approach consists in computing the singular value decompositions of  $\mathbf{U}$  and  $\mathbf{V}$ . As outlined in subsection 4.2, we compute these decompositions by solving generalized eigenvalue problems for  $\mathbf{AY} = \mathbf{U}' * \mathbf{SX} * \mathbf{U}$  and  $\mathbf{AZ} = \mathbf{V}' * \mathbf{SX} * \mathbf{V}$ . In Table 4.3, we summarize the required memory and computational cost for this step. Note that the setup of the

TABLE 4.3

Memory and computation cost for computing and storing  $\mathbf{AY} = \mathbf{U}' * \mathbf{SX} * \mathbf{U}$  and  $\mathbf{AZ} = \mathbf{V}' * \mathbf{SX} * \mathbf{V}$  and the estimated number of operations for the corresponding eigenvalue decompositions. The theoretical complexity estimates here are  $\text{mem}(\mathbf{AY}) = \text{mem}(\mathbf{AZ}) = 8k^2$  bytes,  $\text{ops}(\mathbf{AY}) = \text{ops}(\mathbf{AZ}) = k^2$  flops, and  $\text{ops}(\text{eig}) = O(k^3)$  flops. For the numbers displayed in the table, we use  $\text{ops}(\text{eig}) = 50k^3$  flops.

ref	0	1	2	3	4	5
mem (AX, GB)	0.000	0.000	0.001	0.003	0.015	0.061
ops (AX, Gflop)	0.007	0.113	1.776	28.208	449.699	7 182.205
ops (eig(AX), Gflop)	0.032	0.254	2.031	16.248	129.980	1 039.844

matrices  $\mathbf{AY}$  and  $\mathbf{AZ}$  is more expensive than the corresponding eigenvalue solves, but has the same cost as a single evaluation  $\mathbf{T}(\mathbf{c})$  of the forward operator; cf. Table 4.2.



The additional memory required for storing the  $k \times k$  matrices  $\mathbf{A}\mathbf{Y}$  and  $\mathbf{A}\mathbf{Z}$  is negligible.

The tensor product approximation  $\mathbf{TKK}(\mathbf{c}) = \mathbf{V}\mathbf{K}' * \mathbf{D}(\mathbf{c}) * \mathbf{U}\mathbf{K}$  requires only subblocks  $\mathbf{U}\mathbf{K}$ ,  $\mathbf{V}\mathbf{K}$  of the excitation and emission matrices  $\mathbf{U}$ ,  $\mathbf{V}$  and, therefore, no additional memory cost arises in setting up this approximation. To achieve a  $\delta$ -approximation with  $\delta = 10^{-3}$ , for instance, we expect to require approximately  $K = 100$  singular components of  $\mathbf{U}$  and  $\mathbf{V}$ ; see [Lemma 3.1](#) for details. The tensor product approximation will then have rank  $K^2 = 10^4$ . For the hyperbolic cross approximation  $\mathbf{TK}$ , we however expect to require only approximately  $2K = 200$  components of the tensor product approximation  $\mathbf{TKK}$ ; compare with [Lemma 2.6](#). In [Table 4.4](#) we summarize the expected memory and computational cost for the corresponding approximations. Note that

TABLE 4.4

*Memory and computation cost for storing and applying the tensor product approximation  $\mathbf{TKK}$  of rank  $K^2 = 10^4$  and the corresponding hyperbolic cross approximation  $\mathbf{TK}$  of rank  $2K = 200$ . The theoretical memory and computation cost is given by  $\text{mem}(\mathbf{TKK}) = \text{mem}(\mathbf{TK}) = 16Km$  bytes,  $\text{ops}(\mathbf{TKK}(\mathbf{c})) = Km + K^2m$  flops, and  $\text{ops}(\mathbf{TK}(\mathbf{c})) = 2Km$  flops, respectively.*

ref	0	1	2	3	4	5
mem (GB)	0.001	0.006	0.023	0.009	0.036	1.448
ops ( $\mathbf{TKK}(\mathbf{c})$ , Gflop)	0.009	0.037	0.144	0.574	2.289	9.144
ops ( $\mathbf{TK}(\mathbf{c})$ , Gflop)	0.000	0.001	0.003	0.011	0.045	0.181

the tensor product structure allows to store the tensor product approximation  $\mathbf{TKK}$  as efficiently as the hyperbolic cross approximation  $\mathbf{TK}$ . The application of the latter is, however, substantially more efficient.

The final step in the offline phase consists in the recompression of the intermediate approximations. As before, this is based on singular value decompositions of these operators via solution of generalized eigenvalue problems for the matrices  $\mathbf{BKK} = \mathbf{AKK} * (\mathbf{DD} \setminus \mathbf{AKK})$  respectively  $\mathbf{BK} = \mathbf{AK} * (\mathbf{DD} \setminus \mathbf{AK}')$ , where  $\mathbf{AKK}$  and  $\mathbf{AK}$  are the matrix representations for the operators  $\mathbf{TKK}(\mathbf{c})$  and  $\mathbf{TK}(\mathbf{c})$  respectively; see [subsection 4.2.5](#) for details. The computational cost for the assembly of  $\mathbf{BKK}$  and  $\mathbf{BK}$  is listed in [Table 4.5](#). For an evaluation of the computational complexity, we again assume that  $\mathbf{TKK}$  has rank  $K^2 = 10^4$  and that  $\mathbf{TK}$  is of rank  $2K = 200$ . Let us note that the required mem-

TABLE 4.5

*Complexity for computing  $\mathbf{BKK} = \mathbf{AKK} * (\mathbf{DD} \setminus \mathbf{AKK})$  and  $\mathbf{BK} = \mathbf{AK} * (\mathbf{DD} \setminus \mathbf{AK}')$ . The estimates are  $\text{mem}(\mathbf{BKK}) = 8K^4$  bytes,  $\text{ops}(\mathbf{BKK}) = mK^4$  flops and  $\text{mem}(\mathbf{BK}) = 32K^2$  bytes,  $\text{ops}(\mathbf{BK}) = 2K$  flops.*

ref	0	1	2	3	4	5
ops ( $\mathbf{BKK}$ , Gflop)	92.480	361.44	1 429.1	5 683.4	22 667	90 540
ops ( $\mathbf{BK}$ , Gflop)	0.000	0.001	0.003	0.011	0.045	0.181

ory for storing  $\mathbf{BKK}$  and  $\mathbf{BK}$  is independent of the mesh size; for the setting considered here, it is given by  $\text{mem}(\mathbf{BKK}) = 745\text{MB}$  and  $\text{mem}(\mathbf{BK}) = 0.3\text{MB}$ . Assuming that an eigenvalue decomposition of an  $n \times n$  matrix needs roughly  $\text{ops}(\text{eig}) = 50n^3$  operations, we obtain  $\text{ops}(\text{eig}(\mathbf{BKK})) = 46\,566$  Gflops and  $\text{ops}(\text{eig}(\mathbf{BK})) = 0.373$  Gflops. Even if a computationally more efficient low-rank approximation [\[14, 30\]](#) for the tensor product operator  $\mathbf{TKK}$  would be used, the evaluation of  $\mathbf{TKK}(\mathbf{c})$  remains rather expensive; see [Table 4.4](#) for details. Therefore, the tensor product approximation  $\mathbf{TKK}$  is not really useful for the computation of low-rank approximation on large computational meshes. As indicated by the analysis given in [section 2](#), a quasi-optimal approximation  $\mathbf{TN}$  can be computed also by truncation of the singular value decomposition of the hyperbolic

cross approximation TK, which does not require any additional computations.

**4.4. Inverse problem solution – online phase.** After the construction of the low-rank approximation  $TN(c)$  as outlined above, the actual solution of the inverse problem consists of three basic steps; see [section 1](#) for a brief explanation. The first step is the *data compression* which can be expressed as  $MN=PN*\text{vec}((QmK'*M)*QxK)$ . Here we make explicit use of the tensor product structure, which allows us to efficiently compress the data already during recording. After this, only the second projection  $PN$  has to be applied. The memory and operation cost of the data compression step is summarized in [Table 4.6](#). The additional memory cost is given in MB and thus

TABLE 4.6

*Memory and operation cost for computing the projected data  $MKK = QmK'*M*QxK$ . The estimates are  $\text{mem}(QxK)=\text{mem}(QmK)=\text{mem}(QmK'*M) = Kk$  bytes and  $\text{ops}(MKK)=K^2k + Kk^2$ .*

ref	0	1	2	3	4	5
mem(QxK, MB)	0.067	0.134	0.269	0.537	1.074	2.148
ops (MKK, Gflop)	0.002	0.005	0.015	0.054	0.202	0.783

negligible. Note that the cost for storing the full data  $M$  is  $\text{mem}(M) = k^2$  which is substantially higher. As mentioned before, the data can be partially compressed already during recording, such that access to the full data is actually never required.

The final compression  $MN=PN*MKK$  is independent of the system dimensions  $m, k$  and its computational cost is therefore negligible. The same applies for the solution of the regularized inverse problem  $\text{zadN}=(AN\text{Ant}+\alpha*I)\backslash MN$ , which is the second step in the online phase and only depends on the dimension  $N$  of the reduced model.

The synthesis of the solution according to [\(1.7\)](#) can finally be realized by simple multiplication  $\text{cadN}=\text{Ant}*\text{zadN}$ , where  $\text{Ant}$  denotes the matrix representation of the adjoint of the fully reduced forward operator  $TN$ . The corresponding memory and operation costs are summarized in [Table 4.7](#). As claimed in the introduction, the

TABLE 4.7

*Memory and operation cost for synthesis step  $\text{cadN} = \text{Ant}*\text{zadN}$ . The theoretical estimates for the complexity are here given by  $\text{mem}(\text{Ant})=8mN$  bytes and  $\text{ops}(\text{cadN})=mN$  flops.*

ref	0	1	2	3	4	5
mem(Ant, GB)	0.001	0.003	0.011	0.045	0.181	0.724
ops (cadN, Gflop)	0.000	0.000	0.001	0.006	0.023	0.091

most compute intensive part of the online phase is the data compression, even if the tensor product structure is utilized to compress the data already during recording.

**4.5. Computational results.** The practical performance of our two-step model reduction approach will now be illustrated by comparison to model reduction using truncated singular valued decomposition of the forward operator, and to traditional iterative methods for solving the inverse problem [\(1.1\)–\(1.2\)](#).

The model parameters are set to  $\kappa_x = 1$ ,  $\mu_x = 0.2$ ,  $\rho_x = 10$  and  $\kappa_m = 2$ ,  $\mu_m = 0.1$ , and  $\rho_m = 10$ . We further assume prior knowledge that  $c$  is supported in a circle of radius 0.9, i.e., the distance of its support to the boundary  $\partial\Omega$  is at least 0.1. The singular values of the operators  $\mathcal{U}$  and  $\mathcal{V}$  as well as of  $\mathcal{T}$  can thus be assumed to decay exponentially. The noise level in [\(1.3\)](#) is set to  $\delta = 10^{-5}$  and the regularization parameter  $\alpha$  is chosen from  $\{10^{-n}\}$  via the discrepancy principle. In all

our computations, this led to  $\alpha = 10^{-8}$  which complies to the theoretical prediction for exponentially ill-posed problems [9].

A snapshot of the geometry, the exact solution, and a typical reconstruction is depicted in Figure 4.1. All computations are performed on a workstation with Intel(R) Xeon(R) Gold 6130 CPU @ 2.10GHz and 768GB of memory. In our tests we use only a single core of the processor and an implementation in MATLAB 9.6.0.

**4.5.1. Problem initialization.** This step consists of setting up the excitation and emission matrices  $\mathbf{U}$ ,  $\mathbf{V}$ , which are required for the efficient evaluation of  $\mathbf{T}(\mathbf{c})$ . In Table 4.8, we also report about the singular value decomposition of  $\mathbf{U}$  and  $\mathbf{V}$ , by which we orthogonalize the sources and detectors; as mentioned in subsection 4.3, this is required for computation of the Hilbert-Schmidt norm of the measurements. Recall that the theoretical complexity of the first and third step is somewhat smaller

TABLE 4.8  
Computation times (sec) for the individual steps in the problem setup phase.

ref	0	1	2	3	4	5
initialization of $\mathbf{U}$ , $\mathbf{V}$	0.01	0.06	0.34	3.45	47.74	612.63
setup of $\mathbf{U}' * \mathbf{DX} * \mathbf{U}$ , $\mathbf{V}' * \mathbf{DX} * \mathbf{V}$	0.00	0.01	0.16	2.24	30.68	460.13
eigenvalue decompositions	0.01	0.03	0.24	2.15	33.44	470.88
orthogonalization of $\mathbf{U}$ , $\mathbf{V}$	0.00	0.02	0.09	1.70	25.12	363.64

than that of the second and fourth step. Further note that all computations can be done in the offline phase and their results are required for all further numerical tests, independent of the solution strategy that is used.

**4.5.2. Model reduction – offline phase.** The singular values computed in the decompositions of  $\mathbf{U}$  and  $\mathbf{V}$  allow to determine the truncation indices  $\mathbf{xK}$  and  $\mathbf{mK}$  used to define the  $\delta$ -approximations  $\mathbf{UK} = \mathbf{U}(:, \mathbf{xKK})$  and  $\mathbf{VK} = \mathbf{V}(:, \mathbf{mKK})$ . The length of  $\mathbf{xK}$  and  $\mathbf{mK}$  obtained in our numerical tests are depicted in Table 4.9. On the coarsest

TABLE 4.9  
Truncation indices  $\mathbf{xK}$  and  $\mathbf{mK}$  guaranteeing  $\|\mathbf{U} - \mathbf{UK}\| \leq \delta$  and  $\|\mathbf{V} - \mathbf{VK}\| \leq \delta$  with  $\delta = 10^{-5}$ .

ref	0	1	2	3	4	5
$\mathbf{xK}$	88	139	163	179	185	187
$\mathbf{mK}$	88	121	133	137	137	137

mesh, the number of possible excitations and detectors is limited by the number of boundary vertices, but otherwise, the number of truncation indices  $\mathbf{xK}$  and  $\mathbf{mK}$  are almost independent of the truth approximation. This can be expected since the eigenvalues converge with increasing refinement of the mesh.

**Forward evaluation.** As outlined in subsection 4.3, the full operator and its tensor product approximation can now be simply defined by  $\mathbf{T} = \mathbf{Q}(\mathbf{c}) \mathbf{V}' * \mathbf{D}(\mathbf{c}) * \mathbf{U}$  and  $\mathbf{TKK} = \mathbf{Q}(\mathbf{c}) \mathbf{VK}' * \mathbf{D}(\mathbf{c}) * \mathbf{UK}$ . In Table 4.10, we report about the computation times for a single evaluation of these operators. As can be seen, even the problem adapted evaluation of the full operator  $\mathbf{T}(\mathbf{c})$  becomes practically useless for the solution of the inverse problem (1.1). The tensor product approximation  $\mathbf{TKK}(\mathbf{c})$  seems somewhat better suited but, as we will see below, is still not quite appropriate for the efficient solution of the inverse problem.

TABLE 4.10

*Computation times (sec) for a single evaluation of  $T(c)$  and  $TKK(c)$ .*

ref	0	1	2	3	4	5
$T(c)$	0.00	0.01	0.07	1.03	13.99	214.20
$TKK(c)$	0.00	0.01	0.02	0.11	0.52	2.20

**Truncated singular value decomposition.** As a next step, we consider the low-rank approximation of  $T(c)$  and  $TKK(c)$  by truncated singular value decomposition. For the computation of these decompositions, we consider eigenvalue problems for the symmetric operators  $T(Tt(M))$  and  $TKK(TKKt(MK))$ , which are solved numerically by the `eigs` routine of MATLAB and only require the application of the operators  $T(c)$ ,  $TKK(c)$  and their adjoints  $Tt(M)$ ,  $TKKt(M)$ . The sum of `xK` and `mK` specifies the maximal number of eigenvalues to be considered by the algorithm. In Table 4.11, we display the computation times for eigenvalue solvers and the number  $N$  of relevant eigenvalues required to obtain a  $\delta$ -approximation. The computation times for the decomposition

TABLE 4.11

*Computation times and truncation indices for singular value decompositions for  $T(c)$  and  $TKK(c)$ .*

ref	0	1	2	3	4	5
svd( $T$ )	6.46	28.23	284.33	—	—	—
$N(T)$	231	303	473	—	—	—
svd( $TKK$ )	6.45	15.05	48.40	248.42	994.66	—
$N(TKKt)$	231	276	296	310	314	—

of the full operator  $T$  increase roughly by a factor of 8 per refinement, while those for the tensor product approximation only increase by a factor of 4. Computations taking longer than 1000sec were not conducted. Due to the substantially smaller rank, the evaluation  $TN(c)$  of the low-rank approximations resulting from one of the singular value decompositions above is faster by a factor of more than 100 compared to that of the tensor product approximation  $TKK(c)$ , and even on the finest mesh only takes about 0.01sec.

**Hyperbolic cross approximation and recompression.** As illustrated by our theoretical considerations, we can utilize the hyperbolic cross approximation  $TK$  in the recompression step to bypass the computation of the singular value decomposition of the tensor product approximation  $TKK$  without losing the  $\delta$ -approximation property. In Table 4.12, we summarize the computation times for assembling the hyperbolic cross approximation and the subsequent singular value decomposition for the recompression step. Note that the setup cost for the hyperbolic cross approximation

TABLE 4.12

*Computation times for construction of the hyperbolic cross approximation  $TK(c)$  and its singular value decomposition used for constructing the final approximation  $TN(c)$  with rank  $N(TK)$ .*

ref	0	1	2	3	4	5
setup of $TK$ , $TKTKt$	0.01	0.013	1.38	6.31	30.48	140.32
$K(TK)$	403	933	1 725	1 867	1 905	1 917
svd( $TK$ )	0.08	0.87	2.57	3.51	3.87	4.03
$N(TK)$	166	266	391	396	401	403

increases roughly by a factor of 4 for each refinement, while the subsequent singular value decomposition and the ranks are essentially independent of the mesh level.

Due to the moderate rank  $K(\text{TK})$  of the hyperbolic cross approximation, it pays off to compute the matrix approximation of  $\text{TKTKt}$  and to use it for the subsequent eigenvalue decomposition. As can be seen from Table 4.12, the recompression step allows to reduce the rank by another factor of about 5. As predicted by our theoretical investigations, the rank of the final approximation  $\text{TN}$  is comparable to that of the truncated singular value decomposition of the full operator  $\text{T}$  or its tensor product approximation  $\text{TKK}$ ; cf. Table 4.11. The use of the hyperbolic cross approximation  $\text{TK}$  instead of the full operator or its tensor product approximation however allows to speed up the computation of the final low-rank approximation  $\text{TN}$  substantially. Again, the rank of the approximation becomes essentially independent of the mesh after some initial refinements, reflecting the mesh-independence of our approach.

**4.5.3. Solution of inverse problem – online phase.** We now turn to the online phase of the solution process. Iterative methods are used for the solution of the inverse problem with the full operator  $\text{T}$  and its tensor product approximation  $\text{TKK}$ . As mentioned before, the regularization parameter is set to  $\alpha = 10^{-8}$ , and we use MATLAB’s `pcg` routine with tolerance set to `tol` =  $\alpha\delta^2$ .

In Table 4.13, we display the solution times and the error  $\mathbf{err} = \|c_\alpha^\delta - c^\dagger\|$  obtained for the final iterate. Approximately 1 800 iterations are required for the iterative

TABLE 4.13  
Computation times (sec) and error  $\|c_\alpha^\delta - c^\dagger\|$  obtained for iterative solution of Tikhonov regularization (1.4) with full operator  $\text{T}(\mathbf{c})$  and the tensor product approximation  $\text{TKK}(\mathbf{c})$ .

ref	0	1	2	3	4	5
time(T)	1.24	13.91	320.73	—	—	—
err(T)	0.107	0.106	0.106	—	—	—
time(TKK)	1.22	10.07	65.02	382.76	—	—
err(TKK)	0.107	0.106	0.106	0.106	—	—

solution of (1.4) in all tests, which again illustrates the mesh-independence of the proposed algorithms. Also note that the reconstructions of the computation with the full operator and the tensor product approximation have the same quality, as predicted by our theoretical considerations. Even for the tensor product approximation, the iterative solution for fine meshes is practically infeasible.

We therefore turn now to the numerical solution with the low-rank approximations constructed via hyperbolic cross approximation and recompression. In Table 4.14 we separately list the computation times for the individual steps in (1.7), namely the data compression, the solution of the regularized normal equations, and the synthesis of the reconstruction. Similar online computation times are also obtained for the low-rank approximation computed by truncated singular value decomposition of the full operator  $\mathcal{T}$ , since its rank and approximation properties are very similar to that of the approximation constructed by our approach.

As announced in the introduction and predicted by our complexity estimates, the data compression step becomes the most compute-intensive task in the online solution via the low-rank reduced order model  $\text{TN}$ . While the data compression and synthesis step depend on the dimension of the truth approximation, the solution of the regularized normal equations becomes completely independent of the computational mesh. Also observe that the quality of the reconstruction is not degraded by the use

TABLE 4.14

Computation times (sec) for the individual steps of the inverse problem solution via the proposed reduced order models. For validation of the results, we also list the reconstruction errors  $\|c_\alpha^d - c^\dagger\|$ .

ref	0	1	2	3	4	5
data compression	0.001	0.005	0.028	0.114	0.457	1.831
regularized normal equations	0.002	0.001	0.002	0.003	0.003	0.003
synthesis	0.001	0.001	0.004	0.015	0.061	0.107
reconstruction error	0.112	0.108	0.107	0.107	0.107	0.107

of a low-rank approximation in the solution process. Overall, we thus obtained an extremely efficient, stable, and accurate reconstruction for fluorescence tomography.

**5. Summary.** A novel approach towards the systematic construction of approximations for high dimensional linear inverse problems with operator valued data was proposed yielding certified reduced order models of quasi-optimal rank. The approach was fully analyzed in a functional analytic setting and the theoretical results were illustrated by an application to fluorescence optical tomography. The main advantages of our approach, compared to more conventional low-rank approximations, lies in the vastly improved setup time as well as in the possibility to partially compress the data already during recording, such that the access to the full data is never required.

The most compute intensive part in the offline phase consists in the setup of the discrete representations for  $\mathcal{U}$  and  $\mathcal{V}$  as well as their eigenvalue decomposition. A closer investigation and the use of parallel computation could certainly further improve the computation times for this step. Further acceleration of the data compression and synthesis step could probably be achieved by using computer graphics hardware. The low-dimensional reduced order models obtained in this paper may also serve as preconditioners for the iterative solution of related nonlinear inverse problems, which would substantially increase the field of potential applications.

**Acknowledgments.** The work of the second author was supported by the German Research Foundation (DFG) via grants TRR 146 C3 and TRR 154 C04 and via the “Center for Computational Engineering” at TU Darmstadt.

## REFERENCES

- [1] S. R. ARRIDGE AND J. C. SCHOTLAND, *Optical tomography: forward and inverse problems*, Inverse Problems, 25 (2009), p. 123010, <https://doi.org/10.1088/0266-5611/25/12/123010>.
- [2] A. B. BAKUSHINSKY AND M. Y. KOKURIN, *Iterative Methods for Approximate Solution of Inverse Problems*, Springer, Dordrecht, 2004, <https://doi.org/10.1007/978-1-4020-3122-9>.
- [3] P. BENNER, S. GUGERCIN, AND K. WILLCOX, *A survey of projection-based model reduction methods for parametric dynamical systems*, SIAM Review, 57 (2015), pp. 483–531, <https://doi.org/10.1137/130932715>.
- [4] S. C. BRENNER AND L. R. SCOTT, *The Mathematical Theory of Finite Element Methods*, Springer New York, New York, NY, 2008, <https://doi.org/10.1007/978-0-387-75934-0>.
- [5] S. CHAILLAT AND G. BIROS, *FaIMS: A fast algorithm for the inverse medium problem with multiple frequencies and multiple sources for the scalar Helmholtz equation*, J. Comput. Phys., 231 (2012), pp. 4403 – 4421, <https://doi.org/10.1016/j.jcp.2012.02.006>.
- [6] D. COLTON AND R. KRESS, *Inverse acoustic and electromagnetic scattering theory. 4th ed.*, Springer, Cham, 2019, <https://doi.org/10.1007/978-3-030-30351-8>.
- [7] D. DŨNG, V. TEMLYAKOV, AND T. ULLRICH, *Hyperbolic cross approximation*, Birkhäuser/Springer, Cham, 2018.
- [8] H. EGGER, M. FREIBERGER, AND M. SCHLOTTBOM, *On forward and inverse models in fluorescence diffuse optical tomography*, Inverse Problems and Imaging, 4 (2010), pp. 411–427,



- <https://doi.org/10.3934/ipi.2010.4.411>.
- [9] H. W. ENGL, M. HANKE, AND A. NEUBAUER, *Regularization of inverse problems*, Kluwer Academic Publishers Group, Dordrecht, 1996.
  - [10] L. C. EVANS, *Partial differential equations*. 2nd ed., AMS, 2010.
  - [11] M. FREIBERGER, H. EGGER, M. LIEBMANN, AND H. SCHARFETTER, *High-performance image reconstruction in fluorescence tomography on desktop computers and graphics hardware*, Biomed. Opt. Express, 2 (2011), pp. 3207–3222, <https://doi.org/10.1364/BOE.2.003207>.
  - [12] G. H. GOLUB AND C. F. VAN LOAN, *Matrix computations*. 4th ed., Johns Hopkins University Press, Baltimore, MD, 2013.
  - [13] N. GRINBERG AND A. KIRSCH, *The Factorization Method for Inverse Problems*, vol. 36 of Oxford Lecture Series in Mathematics and its Applications, Oxford University Press, New York, 2008.
  - [14] N. HALKO, P. G. MARTINSSON, AND J. A. TROPP, *Finding Structure with Randomness: Probabilistic Algorithms for Constructing Approximate Matrix Decompositions*, SIAM Review, 53 (2011), pp. 217–288, <https://doi.org/10.1137/090771806>.
  - [15] F. J. HERRMANN, Y. A. ERLANGGA, AND T. T. LIN, *Compressive simultaneous full-waveform simulation*, Geophysics, 74 (2009), pp. A35–A40, <https://doi.org/10.1190/1.3115122>.
  - [16] M. E. HOCHSTENBACH, *A Jacobi–Davidson type SVD method*, SIAM Journal on Scientific Computing, 23 (2001), pp. 606–628, <https://doi.org/10.1137/S1064827500372973>.
  - [17] T. KATO, *Perturbation theory for linear operators*, Springer Berlin Heidelberg, 1966, <https://doi.org/10.1007/978-3-662-12678-3>.
  - [18] T. G. KOLDA AND B. W. BADER, *Tensor decompositions and applications*, SIAM Review, 51 (2009), pp. 455–500, <https://doi.org/10.1137/07070111X>.
  - [19] J. R. KREBS, J. E. ANDERSON, D. HINKLEY, R. NEELAMANI, S. LEE, A. BAUMSTEIN, AND M.-D. LACASSE, *Fast full-wavefield seismic inversion using encoded sources*, Geophysics, 74 (2009), pp. WCC177–WCC188, <https://doi.org/10.1190/1.3230502>.
  - [20] H. W. LEVINSON AND V. A. MARKEL, *Solution of the nonlinear inverse scattering problem by t-matrix completion. i. theory*, Phys. Rev. E, 94 (2016), p. 043317, <https://doi.org/10.1103/PhysRevE.94.043317>.
  - [21] V. A. MARKEL, H. LEVINSON, AND J. C. SCHOTLAND, *Fast linear inversion for highly overdetermined inverse scattering problems*, Inverse Problems, 35 (2019), pp. 124002, 22, <https://doi.org/10.1088/1361-6420/ab44e7>.
  - [22] V. A. MARKEL, V. MITAL, AND J. C. SCHOTLAND, *Inverse problem in optical diffusion tomography iii inversion formulas and singular-value decomposition*, Journal of the Optical Society of America A, 20 (2003), p. 890, <https://doi.org/10.1364/josaa.20.000890>.
  - [23] C. MUSCO AND C. MUSCO, *Randomized block Krylov methods for stronger and faster approximate singular value decomposition*, in Advances in Neural Information Processing Systems 28, C. Cortes, N. D. Lawrence, D. D. Lee, M. Sugiyama, and R. Garnett, eds., Curran Associates, Inc., 2015, pp. 1396–1404.
  - [24] A. NEUBAUER, *An a posteriori parameter choice for Tikhonov regularization in the presence of modeling error*, Applied Numerical Mathematics, 4 (1988), pp. 507–519, [https://doi.org/10.1016/0168-9274\(88\)90013-x](https://doi.org/10.1016/0168-9274(88)90013-x).
  - [25] V. NTZIACHRISTOS, *Fluorescence molecular imaging*, Annual Review of Biomedical Engineering, 8 (2006), pp. 1–33, <https://doi.org/10.1146/annurev.bioeng.8.061505.095831>.
  - [26] F. PUKELSHEIM, *Optimal Design of Experiments (Classics in Applied Mathematics) (Classics in Applied Mathematics, 50)*, Society for Industrial and Applied Mathematics, USA, 2006.
  - [27] A. QUARTERONI, A. MANZONI, AND F. NEGRI, *Reduced basis methods for partial differential equations*, Springer, Cham, 2016, <https://doi.org/10.1007/978-3-319-15431-2>.
  - [28] F. ROOSTA-KHORASANI, K. VAN DEN DOEL, AND U. ASCHER, *Stochastic algorithms for inverse problems involving PDEs and many measurements*, SIAM Journal on Scientific Computing, 36 (2014), pp. S3–S22, <https://doi.org/10.1137/130922756>.
  - [29] E. SOMERSALO, D. ISAACSON, AND M. CHENEY, *A linearized inverse boundary value problem for Maxwell’s equations*, Journal of Computational and Applied Mathematics, 42 (1992), pp. 123 – 136, [https://doi.org/10.1016/0377-0427\(92\)90167-V](https://doi.org/10.1016/0377-0427(92)90167-V).
  - [30] M. STOLL, *A Krylov–Schur approach to the truncated SVD*, Linear Algebra and its Applications, 436 (2012), pp. 2795 – 2806, <https://doi.org/10.1016/j.laa.2011.07.022>.
  - [31] K. VAN DEN DOEL AND U. M. ASCHER, *Adaptive and stochastic algorithms for electrical impedance tomography and DC resistivity problems with piecewise constant solutions and many measurements*, SIAM Journal on Scientific Computing, 34 (2012), pp. A185–A205, <https://doi.org/10.1137/110826692>.